Host metabolic pathways essential for malaria and related hemoparasites in the infection of nucleated cells

Marina Maurizio[1,*], Maria Masid[2,3,*], Kerry Woods[1], Reto Caldelari[4], John G. Doench[5], Arunasalam Naguleswaran[1], Denis Joly[3], Martín González Fernández[1], Jonas Zemp[1,4], Mélanie Borteele[3], Vassily Hatzimanikatis[3], Volker Heussler[4], Sven Rottenberg[1,#], Philipp Olias[1,6,7,#]

[1]Institute of Animal Pathology, Vetsuisse Faculty, University of Bern, Bern, Switzerland

[2]Ludwig Institute for Cancer Research, Department of Oncology, University of Lausanne and Lausanne University Teaching Hospital (CHUV), Switzerland

[3]Laboratory of Computational Systems Biotechnology, École Polytechnique Fédérale de Lausanne (EPFL), Lausanne, Switzerland

[4]Institute of Cell Biology, University of Bern, Bern, Switzerland

[5]Broad Institute of MIT and Harvard, Cambridge, Massachusetts, USA

[6]Institute of Veterinary Pathology, Justus Liebig University, Giessen, Germany

[7]Lead contact

*These authors contributed equally

[#]Corresponding authors (sven.rottenberg@unibe.ch; philipp.olias@vetmed.uni-giessen.de)

SUMMARY

Apicomplexan parasite diseases, including malaria (*Plasmodium*) and theileriosis (*Theileria*), pose a significant threat to global health and the socioeconomic well-being of low-income countries. Despite recent advances, the common host metabolic proteins essential for these highly auxotrophic pathogens remain elusive. Here, we present a comprehensive investigation integrating a metabolic model of *P. falciparum* parasites in hepatocytes and a genome-wide CRISPR screen targeting *Theileria* schizont-infected macrophages. We reveal unifying host metabolic enzymes critical for the intracellular survival of these related hematozoa. We show that pathways such as host purine and heme biosynthesis are essential for both *Theileria* survival and *Plasmodium* liver development, while genes involved in glutathione and polyamine biosynthesis are predicted to be essential for *Plasmodium* only under certain metabolic conditions. Our work highlights the importance of host porphyrins for the viability of liver-stage *Plasmodium*. Shared parasite vulnerabilities provide a resource for exploring alternative therapeutic approaches to combat these crippling diseases.

Keywords: malaria, hematozoa, theileriosis, blood, cattle, cow, Apicomplexa, protozoa, metabolome, drug discovery

INTRODUCTION

Apicomplexa are a large group of unicellular parasites, with more than 6,000 described species and an estimated million(s) yet to be identified.[1] The obligate intracellular organisms can cause severe and life-threatening diseases in humans and animals, of which malaria and theileriosis are particularly devastating. Malaria-causing *Plasmodium* is the most impactful human parasite, with over 245 million malaria cases and more than 600,000 deaths reported annually.[2] Another socio-economically important apicomplexan is *Theileria*, which infects cattle and causes fatal tropical theileriosis (*T. annulata*) in the Middle East and Asia, and east coast fever (*T. parva*) in sub-Saharan Africa.[3-6] *Theileria* parasites have the unique ability among eukaryotic pathogens to induce cancer-like transformation of invaded cells, characterized by sustained proliferation, invasiveness, and altered metabolism.[7,8]

A hallmark of all apicomplexans is that they are auxotrophic for multiple metabolites that need to be taken up from the extra-parasitic environment. This requires complex interactions with the host cell and manipulation of key biological processes.[9-11] Our knowledge of the host metabolic proteins that are essential for the efficient development of these protozoa in their intracellular niche is still very limited. We hypothesized that apicomplexans belonging to different genera rely on shared host metabolic proteins for their development and intracellular survival, and that direct targeting of the host cell and nutrient uptake mechanisms could provide opportunities for new drug development or repurposing. To investigate whether there is an overlap in key host metabolic pathways, we focused on what are arguably the two most important genera of hemoparasites, *Plasmodium* and *Theileria*. A common feature of these two parasites is that, unlike other hematozoa (such as related *Babesia*), they undergo a huge expansion within nucleated cells termed schizogony prior to their red blood cell stage. This occurs within hepatocytes (*Plasmodium*) and white blood

cells (*Theileria*). Following this expansion, the parasites develop into large numbers of merozoites that subsequently infect red blood cells.

Reverse genetic screens, using tools such as CRISPR/Cas9 and RNAi, have proven to be highly effective in the identification of fitness-conferring genes for intracellular pathogens. Large-scale CRISPR screens have been applied to study gene function in a wide variety of living systems, including mammalian cells,[12] bacteria,[13] and apicomplexan parasites.[14-16] Only a few large-scale screens have focused on parasite-specific host gene essentiality, including the murine malaria parasite *P. yoelli*, and the zoonotic parasites *Cryptosporidium parvum* and *Toxoplasma gondii*.[17-19] Studies of *P. falciparum* and *Theileria*-infected host cells are still lacking. While *Theileria* schizonts can be studied in cell culture with quantitative proteomics and host genomic technologies, *Plasmodium* schizont infected hepatocytes are technically difficult to study in large numbers, and large-scale host metabolic data on the major malaria causing species, *P. falciparum*, are lacking.

Genome-scale metabolic models (GEMs) have emerged as invaluable tools in computational systems biology, providing a comprehensive and systems-level understanding of cellular metabolism.[20] By integrating genomic, biochemical, and physiological data, these models provide a holistic representation of the cellular metabolic networks.[21] To date, several GEMs have been developed for apicomplexan parasites including *Plasmodium*.[22-24] Advances in genome annotation, enzyme localization, and definition of available substrates have allowed for a more fine-tuned prediction of essential properties and metabolic activities within *Plasmodium* in recent years.[16,25] One of the most powerful applications of GEMs is their ability to investigate gene essentiality for cell survival and function. By simulating the metabolic fluxes and interactions within a cell, the effects of

100 genetic perturbations on cell growth can be systematically analyzed, advancing our
101 fundamental understanding of cellular processes.[26, 27]
102
103 In this study, we combined computational and experimental approaches to investigate the
104 intricate metabolic interactions between apicomplexan parasites and their nucleated host
105 cells. We reconstructed metabolic models to investigate the dependency of the *P. falciparum*
106 liver stages on host metabolic genes. In parallel, we performed a CRISPR/Cas9 drop-out
107 screen using a novel bovine genome-wide library in *T. annulata* schizont-infected
108 macrophages, the life cycle stage most comparable to the *P. falciparum* liver stage. We
109 identified a set of fitness-conferring genes that are required for the survival of infected
110 macrophages but are dispensable for uninfected macrophages. Our results suggest that
111 multiple host cell biosynthesis pathways and specific metabolic proteins are essential for
112 both *Plasmodium* and *Theileria* parasites. Specifically, we found that *Plasmodium* schizonts
113 depend on the host heme biosynthesis pathway to efficiently develop within the liver. These
114 findings provide new insights into the metabolic interactions between apicomplexan
115 parasites and their host cell environment that could be exploited to develop new strategies
116 for the treatment of disease.
117
118 **RESULTS**
119
120 **Modeling host-parasite metabolic interactions**
121 To study the metabolic interactions between the malaria parasite *P. falciparum* and the
122 human hepatocyte, we developed a systems biology approach to reconstruct a metabolic
123 model that integrates information on the metabolism of both the parasite and the specific
124 host cell, and how the parasite scavenges nutrients from the host. We first reconstructed a
125 human hepatocyte-specific metabolic model (**Figure 1A**) by collecting information from the

126 human protein atlas (www.proteinatlas.org)[28] and previous hepatocyte metabolic
127 networks.[29,30] We then used this information to extract all reactions associated with genes
128 expressed in liver cells from the thermodynamically curated human genome-scale model
129 Recon 3D.[31,32] Next, we built a liver-specific *P. falciparum* metabolic model (liver-iPfa) from
130 the genome-scale model iPfa[25] by defining as nutrients for the parasite those metabolites
131 present in the cytosol of the reconstructed hepatocyte model (**Figure 1B**). Subsequently,
132 the liver-iPfa model was used to study the alternative nutritional requirements of the parasite
133 and the utilization of its available biochemical pathways for biomass synthesis and growth.
134 In addition, we introduce the concept of the *parasitosome*, a reaction that summarizes the
135 metabolic interactions of an intracellular parasite within its host cell. The *parasitosome*
136 reaction is formulated by first identifying the metabolic reactions that the parasite needs for
137 growth under given conditions inside the host cell. These reactions are then combined into
138 one single reaction where substrates represent nutrients that the parasite takes up from the
139 host's cytosol, and products represent metabolites that the parasite secretes into the host.
140 Given the biochemistry of the host and the flexibility of the parasite's metabolism to adapt to
141 varying environmental conditions, alternative *parasitosomes* may exist, representing
142 different metabolic states of the parasites (**Figure S1A**). The alternative *parasitosomes* are
143 then integrated into the hepatocyte model creating a host-parasite model that allows us to
144 study the dependency of the *P. falciparum* schizont on the hepatocyte's metabolism (**Figure**
145 **1C**). This approach allows the analysis of possible scenarios of nutrient availability to *P.*
146 *falciparum* once it has infected the hepatocyte, the metabolism used by the parasite to
147 synthesize biomass building blocks under the specific nutritional conditions, and the
148 essentiality of host genes for parasite survival given the different physiological conditions.
149
150

151 **Host-parasite metabolic interactions and adaptation of *P. falciparum*'s metabolism to**
152 **available nutrients**

153 We used our model to investigate two scenarios: a simulation of a parasite in a rich extra-
154 parasitic environment inside the hepatocyte, with access to 165 nutrients (**Figure 2A, Table**
155 **S1** and methods details), and a parasite in a compromised extra-parasitic environment
156 inside the hepatocyte, when only a minimal set of 47 nutrients is available (**Figure 2A, S1B**).
157 We then examined how the parasite utilizes the available nutrients and its own biochemistry
158 to grow in both cases. We found that *P. falciparum* schizonts in a compromised extra-
159 parasitic environment need to engage in more intracellular reactions than parasites that are
160 in a rich environment (**Figures 2B, S2C**). Based on the computational results, when the
161 parasites are in a rich nutritional environment, they take up a greater number of nutrients,
162 including amino acids, saccharides, fatty acids, and nucleotides (**Figures 2C, S2D**).
163 However, when *P. falciparum* finds a compromised environment inside the hepatocyte, the
164 parasites will have to synthesize unavailable metabolites, relying on their own metabolism
165 and engaging intracellular reactions from central carbon pathways, fatty acid metabolism,
166 pyrimidine metabolism and vitamin metabolism (**Figure 2B**), while elevated levels of by-
167 products such as fatty acids and detoxification molecules might be secreted into the
168 hepatocyte's cytosol (**Figure 2C**).

169

170 Host-directed therapies in host-parasite infections are of increasing scientific interest, as
171 they offer promising therapeutic strategies to disrupt the parasite's life cycle, develop
172 effective treatments, and mitigate drug resistance.[33,34] Therefore, we used the reconstructed
173 models to investigate which hepatocyte metabolic genes are essential for *P. falciparum*
174 survival but dispensable for hepatocyte growth. To this end, we performed gene essentiality
175 analyses in the healthy hepatocyte model and in the hepatocyte-*P. falciparum* integrated
176 model (**Figure 2D**). By *in silico* knocking out of each of the 1927 metabolic genes in the

177 hepatocyte model, we computationally identified 55 essential genes for the healthy
178 hepatocyte (**Figure S3A**). We then simulated the knockout of each gene in the hepatocyte-
179 parasite model to investigate the effect on parasite survival. In the case of parasites growing
180 in a rich extra-parasitic environment, 209 hepatocyte genes from 76 metabolic pathways are
181 essential for at least one *parasitosome*, and not for the hepatocyte. Essential pathways
182 include heme synthesis, purine synthesis, glutathione metabolism, urea cycle, tryptophan
183 metabolism, and fatty acid oxidation (**Figure 2E, S2A**). In the case of *P. falciparum* growing
184 in a compromised extra-parasitic environment inside the hepatocyte, we identified 110
185 genes that are essential for at least one *parasitosome* and dispensable for the hepatocyte,
186 belonging to 57 pathways including heme synthesis, purine metabolism, pentose phosphate
187 pathway, and fatty acid metabolism (**Figure 2F, S2B**).
188
189 Interestingly, the availability of nutrients inside the hepatocyte and the metabolic state of the
190 parasite (different *parasitosomes*) result in varying gene essentiality (**Figure S3B-C**),
191 highlighting the flexible way *P. falciparum* can interact with the hepatocyte. This adaptability
192 might allow the parasite to develop drug resistance and is therefore an important factor to
193 consider when looking for drug targets. For example, when *P. falciparum* has access to a
194 rich nutrient environment in the hepatocyte, it relies on the uptake of these nutrients to
195 synthesize biomass precursors, and so host genes of a particular pathway will be essential.
196 This is the case for the host glutathione synthesis genes *GSS*, *GCLC* and *GCLM*, which
197 provide glutathione to the *parasitosomes*. However, *P. falciparum* has its own glutathione
198 synthesis, which is active when glutathione is scarce, as in a compromised extra-parasitic
199 environment of the host cell. Another example is the polyamine synthesis gene *SRM*, which
200 is only essential for 50% of the *parasitosomes*, suggesting that this gene is essential under
201 specific metabolic states of *P. falciparum*. The *parasitosome* approach allowed us to
202 investigate further which metabolic states of the parasite lead to a specific essentiality. To

203 illustrate this, we examined the interactions between hepatocytes and parasites for
204 polyamines (**Figure 2G**). Our results show that *SRM* is essential when *P. falciparum*
205 preferentially takes up spermine, adenosylmethionine (SAM) and 5-methylthioadenosine
206 (5MTA) from the hepatocyte and secretes decarboxylated adenosylmethionine (dcSAM),
207 depending on the hepatocyte polyamine synthesis to produce spermine and clear the
208 parasite by-products (**Figure 2H-I**). However, *P. falciparum* can synthesize spermine from
209 ornithine using its own polyamine synthesis, in which case *SRM* is not essential because
210 the *parasitosomes* preferentially transport ornithine from the hepatocyte, synthesize
211 spermine, and secrete 5MTA into the hepatocyte (**Figure 2H-I**).
212
213 We identified 19 genes that are essential for all *parasitosomes*, meaning that, based on the
214 computational model, these genes are necessary for the survival of *P. falciparum* under all
215 metabolic conditions. Among them, we found genes from the heme synthesis pathway
216 (*HMBS, UROS, UROD, CPOX* and *PPOX*), purine synthesis pathway (*PPAT, GART, PAICS,*
217 *ATIC,* and *PFAS*) and tryptophan metabolism (*AFMID, KYNU, KMO,* and *HAAO*) (**Figure**
218 **S3D**). The other genes found are involved in NAD metabolism (*QPRT*), taurine and
219 hypotaurine metabolism (*CDO1*), pentose phosphate pathway (*RPIA*), extracellular
220 transport (*SLC11A2*), and cholesterol metabolism (*SOAT1*).
221
222 **Genome-wide CRISPR/Cas9 screen in *Theileria annulata* schizont infected host cells**
223 **identifies parasite-specific essential host genes**
224 Although *Plasmodium* parasites are among the most studied pathogens,[35] large-scale
225 experimental studies of the liver stage are underrepresented. *Theileria* parasites also
226 develop into a multinucleated schizont in bovine leukocytes, and this life cycle stage shares
227 many similarities with the developmental *Plasmodium* liver stage. Therefore, we
228 hypothesized that both hematozoans share core host gene dependencies and rely on the

229 corresponding cellular pathways for successful intracellular development. CRISPR/Cas9
230 loss-of-function screens are among the most valuable techniques for these investigations,
231 and the hyperproliferative behavior of *Theileria*-infected cells makes them suitable for large-
232 scale genetic screens. We therefore performed a genome-wide CRISPR/Cas9 dropout
233 screen in *T. annulata*-infected bovine macrophages (TaC12; **Figure 3A**). For this purpose,
234 we generated a CRISPR sgRNA library based on the bovine ARS-UCD1.2 genome
235 (published in 2018) containing, on average, 4 guides per gene, for a total library size of
236 ~80,000 sgRNAs (**Figure 3B**).
237
238 Infected macrophages were transduced with a Cas9 lentiviral construct. Protein expression
239 was validated by Western blotting (**Figure S4A**). We also used a fluorescence based Cas9
240 reporter assay to select for cells expressing active Cas9 (**Figure S4B-C**). The genome-wide
241 screen was performed at a coverage of 500 with three biological replicates (**Figure 3C, S4D-**
242 **E**). Cells were transduced with lentiviruses for 24 h (DAY 1 - DAY 2, **Figure 3A**) aiming to
243 achieve approximately 30% transduction efficiency, and positive cells were then selected
244 with puromycin. We allowed the cells to grow for another four days to achieve optimal
245 depletion of target genes. On DAY 9, one part of the puromycin-resistant cells was harvested
246 (START point) and the other part reseeded to maintain coverage for later DNA extraction.
247 The dropout screen continued for at least 11 passages (4 weeks), with cells kept under
248 selection and reseeded after each passage. At the end of the screen, surviving cells were
249 harvested (END point) and Illumina Next Generation Sequencing was performed to quantify
250 the abundance of sgRNAs at END and START points. Log_2 fold change (LFC) values were
251 generated based on how sgRNAs changed in abundance throughout the screen, and the
252 average LFC of three biological replicates was used for statistical analysis to identify bovine
253 genes that were depleted in the dropout screen. The data were analyzed using a
254 hypergeometric distribution, where gene LFC values were normalized using intergenic and

255 non-targeting controls (**Table S2**) and displayed in a volcano plot (**Figure 3D**). A hit with a
256 LFC < 0 indicates a reduction in cell fitness upon gene inactivation and consequently these
257 cells are less abundant at the end of the screen compared to the beginning. We assessed
258 the functionality of our library using a reference set of essential and non-essential genes
259 identified by Hart and colleagues[36] (**Figure 3E**). The reference genes were highly fitness
260 conferring, while knockout of non-essential genes did not negatively affect TaC12 cell
261 fitness. We then selected a list of ~1,500 genes that significantly reduced cell fitness upon
262 Cas9-mediated inactivation and designed a CRISPR sgRNA sublibrary (increasing the
263 number of sgRNAs from 4 to 10 per gene) (**Figure 3B**) and performed a small-scale screen.
264
265 In this round of validation, we also screened the uninfected bovine macrophage cell line
266 BoMac to identify genes essential for a cell type with a similar genetic background. Small-
267 scale dropout screens were performed in biological triplicates following the protocol of the
268 genome-wide CRISPR screen (**Figure 3A, S4G, I, Table S3**). Principal component analysis
269 (PCA) of log-normalized counts confirmed the similarity of DAY 0 samples for both TaC12
270 and BoMac cell lines, as well as their resemblance to the plasmid DNA library (**Figure 4A)**.
271 The END samples of both cell lines were clearly separated from each other and from the
272 DAY 0 samples. This suggests a divergent behavior of these two cell lines upon knockout
273 out. While TaC12 screening results have a strong correlation among biological replicates,
274 BoMac screens showed a lower replicate reproducibility, indicating a less consistent
275 response in repeated experiments (**Figure 4B**). About 80% of candidate genes were
276 validated as crucial for TaC12 survival (**Figure S4F**). However, 56% of the TaC12
277 *essentialome* is shared with BoMac (**Figure S4H**), suggesting that many of these genes are
278 also involved in core biological processes. By removing the common fitness-conferring
279 genes, we defined a list of 653 host genes that we considered to be the exclusive *Theileria*-
280 infected macrophage *essentialome*, as these hits are dispensable for BoMac survival

281 (**Figure 4C, Table S4**). One hundred genes that scored as non-essential in the genome-
282 wide screen were included in the sublibrary and these grouped together with intergenic and
283 non-targeting controls in both cell lines, highlighting the ability of our CRISPR library to
284 consistently discriminate between essential and non-essential genes (**Figure 4C, Figure S4**
285 **F, H**).
286

287 **Host genes involved in proliferation, cell growth and metabolism are fitness-**
288 **conferring in *Theileria*-infected bovine macrophages**

289 To scrutinize the *Theileria essentialome* consisting of 653 bovine genes (**Table S4**) we
290 performed a Gene Ontology analysis. This revealed numerous biological processes (**Table**
291 **S5**) with a significant enrichment of proteins involved in ribosome biogenesis and assembly
292 (GO:0042254), mRNA metabolism (GO:0016071), RNA processing (GO:0006396),
293 translation (GO:0006412) and cell cycle progression (GO:0022402), highlighting the
294 importance of continuous protein synthesis to cope with the proliferative phenotype induced
295 by *T. annulata*. Genes involved in the host cell metabolism make up 15% of the *Theileria*
296 essentialome, as revealed by STRING analysis (**Figure 4D**), including biosynthesis of
297 isoprenoids (GO:0008299), glycerolipids (GO:0045017), polyamines (GO:0006596),
298 glutathione (GO:0006749), heme (GO:0006783) and ubiquinone (GO:0006744). The
299 tricarboxylic acid cycle is the most enriched metabolic process in our dataset according to
300 KEGG pathway analysis (**Figure S5A**). For example, mitochondrial enzymes such as
301 aconitase (*ACO2*), succinate dehydrogenase (SDH subunits A-D), fumarate hydratase (*FH*),
302 malate dehydrogenase (*MDH2*) and the catalytic subunit of isocitrate dehydrogenase 3
303 (*IDH3A*) are exclusively fitness-conferring for TaC12 (**Figure S5B**). As expected, since the
304 entire phylum of apicomplexan parasites lacks the *de novo* purine biosynthesis pathway, the
305 *Theileria essentialome* contains several genes involved in the biosynthesis of purine
306 precursors (GO:0009167) (**Figures 4D**, **S6A**). Most of these genes catalyze consecutive

307 reactions in the generation of inosine monophosphate, the intracellular precursor of
308 adenosine and guanosine monophosphates (AMP, GMP). Interestingly, while enzymes that
309 convert IMP to AMP are present (*ADSS* and *ADSL*), those deputed to synthesize GMP
310 (*IMPDH* and *GMPS*) are absent, highlighting a specific requirement for adenine nucleotides
311 by infected cells (**Figure S6B**).
312

313 **Host biosynthesis of glutathione, polyamines, and heme is critical for *Theileria***
314 ***annulata*-infected leukocytes**

315 Among the metabolic hits from the *Theileria* screen we selected three pathways for
316 validation by reverse genetics and chemical inhibition. We aimed for metabolic processes
317 that are dispensable for the host and affect *Theileria*-infected cells through interference with
318 the parasite nutrients supply. Within the glutathione biosynthetic pathway, glutathione is a
319 ubiquitous intracellular and extracellular antioxidant tripeptide synthesized by a two-step
320 reaction catalyzed by the heterodimeric enzyme γ-glutamylcysteine synthetase (γ-GCS;
321 *GCLC*, catalytic subunit; *GCLM*, regulatory subunit) and glutathione synthetase (GSS)
322 (**Figure 5A**). In both genome-wide and small-scale screens, perturbation of the *GSS* and
323 *GCLC* significantly reduced the survival of infected cells over time, while uninfected
324 macrophages showed no defect in cell survival (**Figure 5A**). A single CRISPR/Cas9
325 knockout of bovine *GSS* (**Figure 5A**, **S7A**), resulted in a population of BoMac with 58.7%
326 frameshift mutations in the target gene locus, while >90% of TaC12 retained the wild-type
327 *GSS* sequence. This result suggests that TaC12 *GSS* mutants are not viable and undergo
328 cell death upon gene knockout. To support these data, we treated cells for 72 h with different
329 concentrations of buthionine sulfoximine (BSO), a well-established irreversible inhibitor of γ-
330 GCS,[37] and observed that TaC12 were more sensitive than BoMac in the 30 - 100 μM BSO
331 range (**Figures 5A**, **S7C**), confirming the importance of glutathione biosynthesis exclusively
332 for infected cells. Polyamines are molecules derived from amino acids that are important for

333 cell proliferation and protein synthesis. They are important for rapidly proliferating cells.
334 Mammalian cells have a classical forward-directed *polyamine biosynthetic pathway* that
335 produces polyamines from arginine and methionine, but they also can convert spermine
336 back to spermidine and putrescine via a retroconversion pathway (**Figure 5B**). One of the
337 top depleted genes in the TaC12 screen was spermidine synthase (*SRM*), which was
338 dispensable for BoMac (**Figure 5B**). Targeted *SRM* CRISPR mediated knockout resulted in
339 >82% frameshift mutations in BoMacs, while no significant mutations were detected in
340 surviving TaC12 cells (**Figures 5B**, **S7A**). Consistent with this finding we observed that
341 when cells were treated with the nitric oxide donor sodium nitroprusside (SNP), a potent
342 inhibitor of polyamine biosynthesis,[38] TaC12 showed a >70% reduction in cell viability
343 compared to BoMac (**Figures 5B**, **S7D**). Ablation of five out of the eight enzymes (**Figure**
344 **5C**) of the host *heme biosynthetic pathway* negatively affected the fitness of TaC12 cells in
345 the screen, while no phenotype was observed in uninfected macrophages (**Figure 5C**). We
346 selected *HMBS* for further validation. No viable knockout could be achieved in *Theileria*-
347 infected cells, whereas we were able to generate a polyclonal population of BoMac cells that
348 acquired frameshift mutations in the target gene (**Figure 5C**, **S7A**). Treatment with salicylic
349 acid (SA), an inhibitor of FECH,[39] reduced the viability of TaC12 cells by >60%, whereas
350 BoMac viability remained unchanged (**Figure 5C**, **S7E**). Together, these data validate the
351 critical role of the host glutathione, polyamine, and heme biosynthesis in *Theileria*-infected
352 cells.
353

354 ***Plasmodium* and *Theileria* schizont development depend on several shared host**
355 **pathways**

356 *Plasmodium* liver-stage infection remains one of the least characterized but most attractive
357 targets for malaria prevention as it represents a bottleneck in parasite development with only
358 very few parasites arriving and successfully establishing in hepatocytes. Experimental

359 limitations, such as the low infection rate of *Plasmodium,* prompted us to seek an alternative
360 approach to study the host interplay of the hepatic schizont stages of the human malaria
361 parasite and to search for common essential host metabolic pathways of hematozoans. To
362 this end, we focused on the 99 identified metabolic enzymes from the *Theileria essentialome*
363 of *Theileria*-infected cells (**Figure 4D**) and searched for overlaps with *P. falciparum*
364 hepatocyte gene essentiality predictions in a rich and compromised extra-parasitic
365 environment of the host cell, respectively (**Figures 2E-F, 6**). We identified 24 enzymes,
366 including genes encoding mitochondrial complex II subunits (*SDHA*, *SDHB*, *SDHC*, *SDHD*)
367 and genes involved in polyamine (*AMD1*, *SRM*) and glutathione biosynthesis (*GCLC*, *GSS*),
368 as essential for both parasites when *Plasmodium* grows in a rich environment (**Figure 6**).
369 Of these only seven genes, belonging to the heme and purine biosynthetic pathways, were
370 identified as essential for both parasites when *Plasmodium* growth was modelled in a
371 compromised environment (**Figure 2F**). This suggests that when metabolites such as
372 polyamines and glutathione are available for uptake in the host cytosol, *Plasmodium*
373 parasites scavenge these nutrients. However, in the absence of these molecules in a
374 compromised environment, our model suggests that parasite *de novo* biosynthesis is
375 enough to produce sufficient metabolites. Malaria parasites encode all the genes necessary
376 to synthesize both polyamines and glutathione, but would probably save energy by
377 scavenging from the host. On the other hand, all apicomplexans have lost the ability to
378 synthesize purine nucleotides endogenously and rely on the mammalian host as a source
379 of purines[40]. As expected, we found that the host genes of *ATIC*, *GART*, *PFAS* and *PPAT*
380 are highly fitness-conferring for *Theileria* and essential for all *P. falciparum parasitosomes*
381 (**Figure 6**). We also identified the heme biosynthesis pathway, represented by the host
382 genes *CPOX*, *HMBS* and *UROS*, as essential for both parasites under all conditions.
383 Essentiality of the host heme pathway for *Theileria*-transformed macrophages was not
384 surprising since *Theileria* lacks all enzymes of the heme pathway.[41] However, the prediction

385 that host HMBS is essential for the *P. falciparum* was unexpected, since *Plasmodium*
386 possesses the enzymatic machinery for heme biosynthesis.[41]
387
388 **Perturbation of environmental heme pools strongly influences *Plasmodium* schizont**
389 **development**
390 The importance of the host hepatic heme biosynthesis pathway has not been thoroughly
391 investigated for *P. falciparum*, possibly because malaria parasites are considered heme
392 prototrophic eukaryotes.[41] Transcriptomic data of *P. falciparum* liver stages are not available
393 but have been thoroughly studied for the rodent model parasite of *P. berghei*. *P. berghei*
394 heme biosynthesis gene expression data indicate low activity of the endogenous pathway
395 during biomass increase in the liver stage[42] (**Figure 7A**). Interestingly, *Pb*FECH, the enzyme
396 that catalyzes the final step of the pathway, is significantly upregulated, with expression
397 peaking at the late exo-erythrocytic stage (54 & 60 hpi). Previous research has shown that
398 *Pb*FECH knockout parasites grow to only half the size compared to wild-type parasites.[43]
399 This suggests that parasites may use, at least in part, host cell-derived or systemically
400 available porphyrins. Notably, our models suggest that the mammalian heme pathway plays
401 a central role in the development of the *Plasmodium* exoerythrocytic stage, with three heme
402 pathway genes being identified as potentially essential for both *Plasmodium* and *Theileria*.
403 We chose to knock out *HMBS*, the most upstream gene, to inactivate the entire pathway.
404 For the knockout experiment, we used the haploid cell line HAP1 because knockout
405 approaches are very efficient in these cells, and for infection, we used the rodent model
406 parasite *P. berghei* because infectious sporozoites are readily accessible and able to infect
407 HAP1 cells. Successful ablation of *HMBS* and complementation in HAP1 cells was
408 confirmed at both the gene and protein level (**Figures 7B, S7F**). Although HAP1 ΔHMBS
409 cells are unable to synthesize heme *de novo*, they may be able to import extracellular
410 porphyrins. Fetal calf serum (FCS) added to mammalian cell culture medium contains

411 residual concentrations of heme (~1 - 2μM).[44] We therefore depleted heme and could show
412 that clonal *HMBS*-deficient HAP1 cells do not grow in heme-depleted media, and that this
413 growth defect can be restored by hemin supplementation (**Figure 7C**). We then investigated
414 whether *P. berghei* parasites can successfully develop in HAP1 cells with impaired heme
415 metabolism. We infected six individual HAP1 ΔHMBS clones with *P. berghei* sporozoites
416 and compared parasite size at 48 hpi. As predicted by our metabolic model, we observed a
417 defect in intracellular parasite growth, as parasites were significantly smaller compared to
418 those in WT cells (**Figure 7D**). The marked reduction in parasite size was common to all
419 infected ΔHMBS clones. Next, we analyzed parasite growth after *HMBS* complementation.
420 The reduced size phenotype observed in the parental knockout cells was rescued (**Figure**
421 **7E**), indicating that reactivation of the interrupted host heme biosynthetic pathway allows the
422 successful growth of *Plasmodium* parasites.
423
424 **DISCUSSION**
425
426 Apicomplexan parasites, due to their inherent metabolic constraints, rely heavily on
427 scavenging essential metabolites from their hosts.[40,41,45] This intricate metabolic interplay
428 between *Plasmodium* or *Theileria* becomes particularly critical prior to erythrocyte invasion,
429 when the parasites expand extensively within their nucleated host cells. By employing a
430 synergistic approach that combines genome-scale metabolic network modeling of *P.*
431 *falciparum* infected hepatocytes and genome-wide CRISPR/Cas9 screening of *Theileria*-
432 infected macrophages, we have gained critical insights into the shared metabolic
433 dependencies during the early life-cycle stages within the mammalian host, and pinpointed
434 the metabolic genes of the infected host cell that are critical for parasite survival.
435

436 Because the clonal proliferation of *Theileria*-transformed cells makes them ideal for large-
437 scale screens that are difficult to perform in *Plasmodium*-infected hepatocytes, we
438 performed a CRISPR dropout screen in *Theileria*. We identified a set of 653 host genes,
439 referred to as the *Theileria essentialome*, which significantly impact the growth of *Theileria*-
440 infected cells. This resource includes not only genes involved in protein synthesis and cell
441 proliferation, but also comprises a significant enrichment of host metabolic genes. Since the
442 survival of *Theileria*-transformed macrophages depends on the presence of a viable
443 parasite,[46] we infer that much of the *Theileria essentialome*, particularly those genes
444 involved in metabolic processes, is required for parasite survival. Twenty-four host metabolic
445 enzymes of the *Theileria essentialome* (e.g., of the TCA cycle, polyamine, glutathione,
446 heme, and purine biosynthesis) are shared with the predicted *P. falciparum* hepatocyte
447 model (summarized in Figure 6). Of these, seven genes belonging to the heme biosynthesis
448 and purine synthesis pathways were predicted to be essential for *Plasmodium* growth under
449 all modeled metabolic conditions. This highlights the need to consider the parasite's
450 environment, including the host cell cytoplasm and the extracellular milieu surrounding the
451 host cells, when assessing host-parasite metabolic dependencies. For example, our
452 predictions show that *Plasmodium* schizonts preferentially rely on host glutathione and
453 polyamine synthesis in a "rich" nutrient environment but can switch to endogenous synthesis
454 when the availability of metabolites in the host is limited.
455
456 An important metabolite in the glutathione pathway is GSH, which plays a critical role in
457 protecting cells from oxidative stress. *Plasmodium* has an active GSH biosynthetic pathway
458 that is vital for its development in the mosquito. Since *P. berghei* GSS knockout mutants
459 develop efficiently in the liver *in vivo*,[16] this supports our prediction of a preferential
460 dependency on host *GSS*. While *Plasmodium* can potentially rely on its own glutathione
461 synthesis pathway when needed, our data indicate that modulating host GSH levels, in

462 combination with antimalarial therapy, may be a promising line of future research in malaria
463 therapy. Interestingly, knockdown of host *GSS* has previously been reported to increase the
464 susceptibility of human macrophages to the anti-leishmanial activity of glucantime.[47] In
465 addition, targeting GSH in the context of anti-parasite therapy has parallels to anti-cancer
466 therapy, where high GSH levels are also essential for cancer cell survival. Strategies such
467 as inhibiting GSH synthesis by cysteine starvation or targeting of the amino acid antiporter
468 system Xc- and combination treatment with the γ-GCS inhibitor buthionine sulfoximine
469 (BSO) have already shown promise as anti-tumor combination therapies, [48-50] and warrant
470 exploration in the context of malaria and theileriosis therapies.
471
472 Another important finding is the essentiality of host *SRM* for the *Plasmodium* liver stage
473 development, contingent on the environment. Polyamines are essential molecules for all
474 eukaryotes, and *Plasmodium* parasites are unique among apicomplexans in encoding a
475 complete set of enzymes for endogenous polyamine biosynthesis. *Theileria*, on the other
476 hand, is completely auxotrophic for these amines.[51-53] Malaria parasites can synthesize all
477 three major polyamines, including spermine, although their genome lacks an orthologue of
478 the SMS gene.[53] Instead, they encode for a promiscuous SRM enzyme capable of producing
479 spermidine and, to a much lesser extent, spermine.[54] The physiological role of spermine for
480 *Plasmodium* parasites remains unclear, and there is no evidence for an uptake mechanism,
481 also warranting further investigation.
482
483 Our data also reveal the shared dependency of both *Plasmodium* and *Theileria* on four host
484 genes (*ATIC*, *GART*, *PFAS* and *PPAT*) involved in purine synthesis. This observation is
485 consistent with the fact that the entire phylum of Apicomplexan parasites lacks an
486 endogenous purine synthesis pathway, highlighting their dependency on the acquisition of
487 these bases from the mammalian host.[40]

488

489 In contrast, diverse heme acquisition strategies have been described among Apicomplexan
490 parasites. While *Plasmodium* and *Toxoplasma* possess a complete and functional *de novo*
491 heme biosynthetic pathway, parasites such as *Babesia*, *Theileria* and *Cryptosporidium*
492 depend on acquiring heme from the host cell.[41] Our experiments provided insights into the
493 consequences of loss of the host heme pathway in *P. berghei* and confirmed the unexpected
494 predictions of our model. When *HMBS* was compromised, *P. berghei* failed to reach its
495 normal size at 48 hpi. Strikingly, complementation of *HMBS* completely reversed this
496 phenotype. While there are conflicting data regarding the essentiality of *Pb*ALAS in the liver,
497 external ALA could rescue *P. berghei* lacking *ALAS*.[55,56] This is consistent with the idea that
498 liver-stage *Plasmodium* can utilize external ALA for heme synthesis. Rathnapala et al. further
499 demonstrated that FECH-deficient *P. berghei* grew smaller in size during liver stage
500 development.[43] Taken together, this suggests that endogenous heme synthesis becomes
501 critical during liver development, in contrast to the intraerythrocytic stages.[55-58] Our results
502 now add to this picture by suggesting that the host heme synthesis enzymes upstream of
503 FECH play a fitness-conferring role in the parasite development. However, the identity of
504 porphyrin transporters in apicomplexans remains relatively unexplored,[41] and requires
505 further investigation.

506

507 In conclusion, our study has demonstrated the power of integrating computational modeling
508 with experimental approaches to uncover crucial host genes essential for intracellular
509 survival of two of the deadliest parasites on the planet. The methods developed in this study
510 provide an adaptable framework for investigating a range of other host-parasite interactions,
511 allowing a deeper understanding of common host dependencies. Moreover, our findings
512 open up exciting opportunities to simultaneously target both host and parasite pathways and

513 to explore gene essentiality in specific environmental contexts and cellular niches, paving
514 the way for innovative combination therapies against these devastating pathogens.
515

516 **ACKNOWLEDGEMENTS**

517 We thank the Department for BioMedical Research (DBMR) and the Flow Cytometry and
518 Cell Sorting Facility (FCCS) of the University of Bern, Switzerland. Financial support came
519 from the Swiss National Science Foundation (CRSII5_198543, 310030_189127,
520 PZ00P3_173972). Figures were created with the help of BioRender.
521

522 **AUTHOR CONTRIBUTIONS**

523 Conceptualization, KW, SR, PO; methodology, JGD, KW, VHr, VHa, SR, PO; investigation,
524 MMr, MMs, KW, RC, AN, DJ, JZ, MB; formal analysis, MMr, MMs, KW, RC, AN, MGF, PO;
525 writing – original draft, MMr, MMs; writing – review & editing, KW, RC, JGD, AN, VHr, VHa,
526 SR, PO; funding acquisition, VHa, VHr, SR, PO; resources, VHa, VHr, SR, PO; supervision,
527 VHa, VHr, SR, PO
528

529 **DECLARATION OF INTERESTS**

530 The authors declare no competing interests.
531
532

533 **FIGURE LEGENDS**

534

535 **Figure 1. Systems biology workflow to study host-parasite metabolic interactions of**
536 ***Plasmodium falciparum* in the liver.** (**A**) Reconstruction of a hepatocyte-specific model
537 from the human genome-scale metabolic model by integrating omics data. (**B**)
538 Reconstruction of a liver-specific *P. falciparum* metabolic model from the iPfa genome-scale
539 model by restricting the extra-parasite environment to metabolites available in the cytosol of
540 the liver metabolic model. The reconstructed liver-iPfa model is used to analyze the
541 nutritional requirements of the parasites and to formulate *parasitosome* reactions
542 representing different metabolic states that the parasites can acquire to adapt to their
543 environment and synthesize biomass. (**C**) Reconstruction of an integrated host-parasite
544 model, by incorporating the *parasitosome* reactions into the liver metabolic model.

545

546 **Figure 2. Analysis of *P. falciparum* metabolic states and host genes essential for**
547 **parasite growth.** (**A**) Case study I – rich extra-parasitic environment: *P. falciparum* has
548 access to the entire hepatocyte's cytosol metabolome. Case study II – compromised extra-
549 parasitic environment: *P. falciparum* has access to a minimal set of nutrients from the
550 hepatocyte's cytosol. (**B**) Assignment to metabolic subsystems of the reactions that
551 compose the minimal networks for the different *parasitosomes*, when considering a rich
552 (green) or a compromised (orange) extra-parasitic environment (ePE), in terms of number
553 of reactions and percentage of subsystem coverage for selected pathways. (**C**) Metabolic
554 composition of the alternative *parasitosomes* in case study I (rich ePE, green) and II
555 (compromised ePE, orange). *Parasitosomes* are representations of the nutrients taken up
556 from and products secreted to the hepatocyte by parasites in different metabolic states. (**D**)
557 Scheme of gene essentiality analysis performed in the integrated host-parasite model (**E-F**)
558 Hepatocyte genes essential for *P. falciparum* in case study I (rich ePE, green) and in case

559 study II (compromised ePE, orange) for selected pathways. Classification by associated
560 metabolic processes, number of genes, and frequency of essentiality across *parasitosomes*.
561 (**G**) Host-parasite interactions for polyamine synthesis. (**H**) Nutrients used and products
562 secreted by the parasites into the hepatocyte for the polyamine's pathway. Separated into
563 parasites that require the hepatocyte's *SRM* gene for survival (green) and those that survive
564 independently of the host's *SRM* gene (grey). Column divisions group *parasitosomes* with
565 the same metabolic flux profile for the polyamine synthesis (**I**) Activity of the polyamine
566 pathway in *parasitosomes* in relation to their dependence on the host's SRM gene. SAM:
567 adenosylmethionine, dcSAM: decarboxylated SAM, 5MTA: 5-methylthioadenosine.
568
569 **Figure 3. Genome-wide CRISPR/Cas9 screen in *Theileria annulata*-infected bovine**
570 **macrophages identify host factors essential for parasite survival. (A)** Schematic
571 workflow of CRISPR dropout screens. Cas9-expressing infected macrophages (TaC12)
572 were transduced with a pooled CRISPR sgRNA lentiviral library and maintained in culture
573 for at least 11 passages. Genomic DNA was harvested at the START and END points and
574 sgRNA abundance was quantified. The screen was performed in 3 biological replicates. **(B)**
575 Detailed information on the bovine CRISPR/Cas9 libraries used in this study. **(C)** Correlation
576 plot screen replicate. Dark red indicates high similarity between replicates, while dark blue
577 indicates low correlation. **(D)** Volcano plot showing the hypergeometric distribution analysis
578 of the TaC12 genome-wide screen. Each gene is plotted based on its average $\log_2$ fold
579 change (LFC, z-normalized using control dispersion) and the negative $\log_{10}$ of its *p*-value.
580 Intergenic and non-targeting controls are shown in blue and green, respectively. The
581 horizontal dotted line corresponds to *p*-value = 0.05, and the vertical dotted line corresponds
582 to average z-normalized LFC of the controls (intergenic and non-targeting) minus 1x
583 standard deviation of the whole genetic screen. **(E)** Boxplot representing TaC12 genome-

584 wide screen scoring (z-normalized LFC values) of groups of annotated “essential” and “non-
585 essential” genes.
586
587 **Figure 4. Pathway analysis of fitness-conferring host genes for *Theileria* schizonts.**
588 **(A)** Principal component analysis plot of the log-norm counts distribution of each biological
589 replicate of small-scale screens in BoMac and TaC12. Color legend: BoMac_DAY0_r1-2-3
590 (blue), BoMac_END_r1-2-3 (purple), TaC12_DAY0_r1-2-3 (red), TaC12_END_r1-2-3 (sage
591 green), CRISPR sublibrary (neon green). **(B)** Correlation plots of small-scale screen
592 replicates. Dark red indicates high similarity between replicates, while dark blue indicates
593 low correlation. **(C)** Scatter plot showing the results of the small-scale screen. Each gene is
594 plotted based on z-normalized LFC values in infected versus uninfected cells. Genes
595 depleted only in TaC12 cells are colored in light blue. Intergenic and non-targeting controls
596 are shown in orange and green, respectively. One hundred non-essential genes from the
597 TaC12 genome-wide screen are highlighted in orange. Dotted lines correspond to the
598 average z-normalized LFC of the controls (intergenic and non-targeting) minus 1x standard
599 deviation of each genetic screen. **(D)** Protein interaction network and Gene Ontology (GO)
600 analysis of metabolic genes present in the *Theileria essentialome*. The list of 99 metabolic
601 genes was analyzed using the STRING database (https://string-db.org/) on 19 July 2023.
602 Line thickness indicates the strength of data support. Active interaction sources considered:
603 text mining, experiments, databases, co-expression. Only interactions with the highest
604 confidence score are shown. Gene ontology enrichment analysis identified 10 major host
605 metabolic pathways.
606
607 **Figure 5. Host glutathione, polyamine, and heme pathways are essential for *Theileria***
608 **A)** Scoring of *GCLC* and *GSS* in TaC12 vs. BoMac screens. TIDE analysis of *GSS*
609 CRISPR/Cas9 knockout in BoMac and TaC12 cells. Resazurin viability assay showing the

610 percentage of survival of BoMac and TaC12 cells after 72 h treatment with buthionine
611 sulfoximine (BSO), an inhibitor of γ-GCS, as indicated in the schematic of the glutathione
612 biosynthetic pathway. The gene knocked out in TaC12 and BoMac is indicated with delta
613 (Δ) in the pathway. **(B)** Scoring of *AMD1*, *SMS* and *SRM* in TaC12 vs BoMac screens. TIDE
614 analysis of *SRM* CRISPR/Cas9 knockout in BoMac and TaC12 cells. Resazurin viability
615 assay showing the percentage of survival of BoMac and TaC12 cells after 72 h treatment
616 with sodium nitroprusside (SNP), an inhibitor of ODC as indicated in the schematic of the
617 polyamine biosynthetic pathway. The gene knocked out in TaC12 and BoMac is indicated
618 with delta (Δ) in the pathway. **(C)** Scoring of *ALAD*, *HMBS*, *UROS*, *CPOX* and *FECH* in
619 TaC12 vs BoMac screens. TIDE analysis of *HMBS* CRISPR/Cas9 knockout in BoMac and
620 TaC12 cells. Resazurin viability assay showing the percentage of survival of BoMac and
621 TaC12 cells after 72 h treatment with salicylic acid (SA), an inhibitor of FECH as indicated
622 in the schematic of the heme biosynthetic pathway. TIDE and viability experiments were
623 performed in triplicate with similar results (Fig. S4 E-G-H-I). A representative replicate is
624 shown for each. The gene knocked out in TaC12 and BoMac is indicated with delta (Δ) in
625 the pathway.
626
627 **Figure 6. Host metabolic pathways and genes essential for *Plasmodium* and *Theileria***
628 **schizont survival in nucleated host cells.** Venn diagram showing multinucleated parasite
629 schizonts and the overlap between the *Theileria* metabolic essentialome and *P. falciparum*
630 host metabolic gene essentiality predictions in a compromised and rich extra-parasitic
631 environment.
632
633 **Figure 7. Environmental heme from the host cell plays a key role in the development**
634 **of *Plasmodium* exo-erythrocytic schizonts. (A)** Expression of *P. berghei* heme
635 biosynthesis genes throughout the parasite's life cycle. Most parasite genes are expressed

636 at low levels during the liver stage (EEF), except for *FECH*. EEF, exo-erythrocytic form; DC,
637 detached mammalian cell containing merosomes. (**B)** Western blot of whole cell lysates from
638 HAP1 wild type, ΔHMBS clone (cl.) A, and a pool of ΔHMBS cl. A::HMBS complemented
639 cells. Tubulin was used as a loading control. **(C)** Phase contrast images of HAP1 wild type
640 and HAP1 ΔHMBS cl. A after 48 h incubation in normal 10% FCS-IMD media, heme-
641 depleted 10% FCS-IMDM, and the latter with hemin supplementation. **(D)** *P. berghei* exo-
642 erythrocytic schizont size at 48 h pi in HAP1 WT and six HAP1 ΔHMBS clones A - F. **(E)**
643 Parasite size at 48 hpi in HAP1 WT, ΔHMBS cl. A, and ΔHMBS cl. A::HMBS
644 complementation. *P*-values are shown in D and E.
645

646 # STAR ★ METHODS

647

648 ## KEY RESOURCES TABLE

REAGENT or RESOURCE	SOURCE	IDENTIFIER
Deposited Data		
Human GEM Recon 3	Brunk et al, 2018	https://www.vmh.life
Thermodynamically curated GEM Recon 3D	Masid et al. 2020	https://github.com/EPFL-LCSB/redhuman
Human protein data	The Human Protein Atlas	https://www.proteinatlas.org/
Fluxomics data for hepatocyte model	Agren et al. 2014	doi:10.1002/msb.145122
Metabolomics data for hepatocyte model	Gille, Bolling, Hoppe, et al. 2010	doi:10.1038/msb.2010.62
Experimental Models: Cell Lines		
TaC12	Shiels et al., 1992	doi:10.1242/jcs.101.1.99
BoMac	Stabel et al., 1995	doi:10.1016/0165-2427(94)05348-v
HAP1	Carette et al., 2011	doi:10.1038/nbt.1857
Software and Algorithms		
MATLAB	MathWorks	R2021b
CPLEX	IBM	CPLEX Optimization Studio V12.10.0
matTFA	Salvy, et al. 2018	https://github.com/EPFL-LCSB/mattfa
lumpGEM	Ataman and Hatzimanikatis, 2017	https://github.com/EPFL-LCSB/redgem
Other		
Repository with code for model reconstruction and metabolic analysis	This paper	https://github.com/EPFL-LCSB/host_parasite_interactions

649

650

651 ## RESOURCE AVAILABILITY

652

653 ### Lead contact

654 Further information and requests for resources and reagents should be directed to the lead

655 contact, Philipp Olias (philipp.olias@vetmed.uni-giessen.de).

656

657

658 **Materials availability**

659 All unique/stable reagents generated in this study are available from the Lead Contact with
660 a completed Materials Transfer Agreement.

661

662 **Data and code availability**

663 The code generated during this study is available at https://github.com/EPFL-
664 LCSB/host_parasite_interactions.

665

666 **METHOD DETAILS**

667

668 **Hepatocyte specific model**

669 Starting with the thermodynamically curated human genome-scale Recon 3D[31,32], we
670 reconstructed a hepatocyte metabolic model by taking into account the physiology of
671 hepatocytes and the genes expressed in liver cells. Towards this end, we defined the
672 physiology of hepatocytes by integrating in the human Recon3D model publicly available
673 fluxomics data for 92 boundary reactions[29] and metabolomics data for 213 metabolites[30]
674 from previous hepatocyte model reconstructions. Additionally, we set a growth rate of the
675 hepatocyte to a maximum of 0.014 h^{-1} corresponding to a doubling time of 49.5 h[59] and the
676 ATP maintenance rate to at least 1.07 mmol/gDW/h[60]. The Human Protein Atlas
677 (www.proteinatlas.org) [28] was used to identify 1853 metabolic genes present in liver cells.
678 By mapping these genes to the Recon 3D reactions (using the gene-protein-reaction rules),
679 5926 reactions conformed the starting core of the hepatocyte model. We then formulated
680 the following MILP to integrate additional reactions required for the core reactions to carry
681 flux:

$$
\begin{array}{lll}
objective\ function & \max \sum_{k=1}^{nc} z_k & \\
 & \text{subject to} & \\
FBA\ constraints & \mathbf{S} \cdot \boldsymbol{v} = \mathbf{0} & \\
 & \boldsymbol{v}_L \leq \boldsymbol{v} \leq \boldsymbol{v}_U & \\
TFA\ constraints & \Delta_r \mathrm{G}_i' = \sum_{j=1}^{m} n_{i,j} \Delta_f \mathrm{G}_j'^{o} + RT \ln\left(\prod_{j=1}^{m} x_j^{n_{i,j}}\right), & i = 1, \dots, n, \\
 & \Delta_r \mathrm{G}_i' - M + M \cdot b_i^F \leq 0 & \\
 & -\Delta_r \mathrm{G}_i' - M + M \cdot b_i^R \leq 0 & \\
 & v_i^{F,R} - M \cdot b_i^{F,R} \leq 0 & \\
 & b_i^F + b_i^R \leq 1 & \\
constraints\ for & b_k^F + b_k^R + C \cdot z_k \leq C, & k = 1, \dots, nc, \\
non-core\ reactions & \boldsymbol{v}_c^F + \boldsymbol{v}_c^R \geq \epsilon, & \forall c \in core
\end{array}
$$

where m is the number of metabolites in the network, n is the number of reactions in the network, nc is the number of non-core reactions, z_k are binary variables for all the non-core reactions, $\mathbf{S}$ is the stoichiometric matrix, $\boldsymbol{v}$ are the net fluxes for all the reactions and v_i^F, v_i^R are the corresponding net-forward and net-reverse fluxes, so that, $v_i = v_i^F - v_i^R$, $for\ all\ i = 1, \dots, n$. $\boldsymbol{v}_L$ and $\boldsymbol{v}_U$ are the lower and upper bound, respectively, for all the reactions in the network. $\Delta_r \mathbf{G}'$ is the Gibb's free energy of the reactions and $\mathbf{b}^F$ and $\mathbf{b}^R$ are the binary variables for the forward or reverse fluxes of all the reactions (coupled to TFA). M is a big constant (bigger than all upper bounds), C is an arbitrary large number, and ϵ a small number. With this formulation, if $z_k = 0$, then reaction k is active.

As a result, the hepatocyte model contained a total of 3899 metabolites, 6209 reactions, and 1927 genes.

Liver-specific model for *Plasmodium falciparum*

The liver-iPfa model is reconstructed from the published iPfa genome-scale model for *P. falciparum*[25] by blocking the reactions that transport in and out of the parasite compounds that are not present in the liver model. By mapping the extra-parasitic metabolites from iPfa

700 to the cytosolic metabolites from the hepatocyte model, we found that from the 241 nutrients
701 that the parasite can transport, 165 (**Table S1**) are present in the cytosol of the liver model.
702 We then blocked the corresponding 76 transport reactions and removed the reactions that
703 could not carry flux in iPfa, resulting in a liver-iPfa model of 737 metabolites, 889 reactions,
704 210 genes, and a growth of 0.073 h-1 (doubling time of 9.48 h).
705

706 **Minimal nutritional requirements for liver-stage *Plasmodium falciparum***

707 In order to investigate the minimal set of nutrients that the liver-stage *P. falciparum* needs to
708 sustain growth, we applied the *in silico minimal medium* (iMM) method[31] to the liver-iPfa
709 model. The iMM method identifies the minimal set of nutrients that are required to satisfy a
710 specific growth rate. In this case, we identified that parasites need a minimum of 31 nutrients
711 to grow. Given the flexibility of the intracellular metabolism to synthesize the required
712 precursors for biomass, there exist alternative sets of nutrients that could serve to achieve
713 the same growth rate. In this case, using iMM we found 1792 alternative sets of 31 nutrients,
714 leading to a total of 47 unique nutrients across sets. By classifying the presence of these
715 nutrients in the corresponding 1792 sets, we identified 23 nutrients that appear in all sets,
716 which we call constitutive, and 24 nutrients that are not appearing systematically in all sets
717 because they can substitute each other, as they contribute with the same backbone
718 moieties.
719

720 **The *parasitosome* as a representation of the metabolic state of *Plasmodium***
721 ***falciparum***

722 The *parasitosomes* are generated using the lumpGEM method[61], setting as objective the
723 biomass reaction. This includes three steps (**Figure S1A**): [62] definition of the extra-parasitic
724 environment in the metabolic model, (2) identification of the minimal number of reactions
725 required for growth, the resulting set of reactions is called minimal network (MiN), and (3)

726 generation of an individual reaction by collapsing all the reactions present in the MiN into
727 one lumped reaction. As a result, the *parasitosome* reaction represents the interactions of
728 the parasite with its environment, containing nutrients as substrates and secretions as
729 products in the stochiometric equation. Given the flexibility of the intracellular metabolism,
730 for the same physiological conditions, several MiNs can exist, representing alternative
731 metabolic pathways that the parasites can use to synthesize the biomass precursors.
732
733 We have formulated *parasitosomes* for the two case studies with rich or compromised extra-
734 parasitic environment (ePE). In the case that a rich ePE is available, a minimum of 248
735 reactions are required and there exist 151 alternative MiNs (**Figure S1C**). By lumping the
736 MiNs into individual reactions, we generated 151 *parasitosomes* that use a total of 75
737 nutrients and secrete a total of 27 products (**Figure S1D**). In the case where the parasite
738 encounters a compromised extra-parasitic environment, the size of the MiNs is 307
739 reactions and there exist 8 alternatives (**Figure S1C**), resulting in 8 alternative
740 *parasitosomes* that take up a total of 36 nutrients and secrete 36 products (**Figure S1D**).
741
742 **Reconstruction of a hepatocyte-parasite integrated metabolic model**
743 The generated *parasitosome* reactions were integrated into the hepatocyte metabolic
744 model. We then evaluated whether the bounds of the transport reactions in the hepatocyte
745 model needed to be modified in order to sustain the growth of both the parasite and the
746 hepatocyte. To do this, we formulated the following MILP:

$$objective\ function \quad \min \sum_{t=1}^{tpt\_rxn} \delta_{L_t} + \delta_{U_t}$$

subject to

$$\begin{array}{lll} & FBA\ constraints & \\ & TFA\ constraints & \\ fix\ biomass & v^F_{biomass_{host}} \geq \rho \cdot \mu_{host} & \\ & v^F_{biomass_{parasite}} \geq \rho \cdot \mu_{parasite} & \\ relax\ bounds & v_{L_t} - \delta_{L_t} \leq v_t \leq v_{U_t} + \delta_{U_t} & \forall t \in tpt\_rxn \end{array}$$

where tpt_rxn is the set of transport reactions in the network, $\boldsymbol{v}$ are the net fluxes for all the reactions and, $\boldsymbol{v}_L$ and $\boldsymbol{v}_U$ are the lower and upper bound, respectively, for all the reactions in the network. $\delta_{L_t}$and δ_{U_t} are the relaxations of the lower and upper bound respectively. μ_{host} and $\mu_{parasite}$ are the theoretical maximum biomass for host and parasite, respectively and, ρ is a percentage (0 - 100%).

As a result, the integrated model contains 3906 metabolites, 6377 reactions, and 1927 genes.

Gene essentiality analysis in the integrated hepatocyte-parasite model

We performed gene essentiality analysis[63] in the healthy hepatocyte model and in the integrated hepatocyte-parasite model. In this analysis, hepatocyte genes are knocked out individually in the network. When a gene encoding for an enzyme is knocked out, the reaction rate is set to zero and we evaluated whether the corresponding KO influences biomass production.

For the integrated hepatocyte-parasite model, we knocked out the hepatocyte genes and we evaluated the impact on biomass production for the hepatocyte and for each individual *parasitosome*. We then selected the genes that were essential for parasite growth but not for hepatocyte biomass production, nor for the healthy hepatocyte.

768

769 **Cell culture**

770 *T. annulata*-infected macrophages (TaC12) were maintained in L15 medium (Gibco, Thermo
771 Fisher Scientific, Waltham MA, USA), while uninfected bovine macrophages (BoMac)[64] and
772 human embryonic kidney cells (HEK293FT) were grown in DMEM medium (Gibco). HAP1
773 cells, a human near-haploid cell line derived from chronic myelogenous leukemia KBM-7
774 cells, were maintained in IMDM medium (Gibco). All media were supplemented with 10%
775 heat-inactivated fetal calf serum (BioConcept, Allschwill, Basel, Switzerland), 2 mM L-
776 glutamine (BioConcept), 10 U/mL penicillin-streptomycin (BioConcept). L15 and DMEM
777 media were also supplemented with 10 mM HEPES pH 7.2 (Merck). All cell lines were grown
778 at 37 °C in an atmosphere containing 5% CO_2, except for TaC12, which were cultured at 0%
779 CO_2.

780

781 **Plasmids**

782 All plasmids used in this study are listed in the Table S6.

Purpose	Plasmid name	Source
Lentivirus production	psPAX2 packaging plasmid	Addgene, #12260
	pMD2-G VSV-G envelope plasmid	Addgene, #12259
Generation of Cas9-expressing cell lines	Cas9-Flag-Blast pXPR_BRD107	Broad Institute
Fluorescence-based reporter assay for selection of Cas9-expressing cells	pKLV2-U6gRNA5(gGFP)-PGKBFP2AGFP-W reporter plasmid	Addgene, #67980
Generation of HAP1 ΔHMBS clones	pCRISPR_v3.1	Modified from Addgene, #62988
Re-expression of HMBS in HAP1 ΔHMBS clone A	pCMV-puroR	Modified from pcDNA4/TO (Invitrogen)

783

784 **Table S6.** Plasmids employed in the study.

785

786 **Human and bovine sgRNAs**

787 All sgRNAs used in this study are listed in the Table S7.

Target gene	sgRNA name	sgRNA sequence (5' – 3')
Human HMBS	hHMBSg1	GCAGCTTGCTCGCATACAGA
Bovine GSS	bGSSg1	GACTCACCGATGCACAGCTG
Bovine SRM	bSRMg1	GGACGGCGTTATCCAGTGCA
Bovine HMBS	bHMBSg1	TCAAGAATCTTGTCCCCCG
Bovine VIM	bVIMg3	AACGACAAAGCCCGCGTCG

788

789 **Table S7**. sgRNAs designed for single CRISPR/Cas9 knockout of candidate genes.

790

791 **Primers**

792 All primers were synthesized by Microsynth AG (Baldach, Switzerland). Primers for plasmids

793 and TIDE PCRs are listed in the Table S8.

Purpose	Sequence (5' – 3')	Orientation
TIDE analysis for bGSSg1	AGAAGAATGATTCCACTGGG	Forward
	ACTAAAGTCCAGCCTTCAAA	Reverse
TIDE analysis for bSRMg1	GCATCCTTCTCGCTGGGCT	Forward
	CAGACACAGCTCCCTGGAAC	Reverse
TIDE analysis for bHMBSg1	TTCTGGACAGGAATGGAAGC	Forward
	AGATCCAGGACTCTCTCCTT	Reverse
TIDE analysis for bVIMg3	CAACACCGAGTTCAAGAACA	Forward
	TTTCTCAAAGTTTGGGGAAA	Reverse
TIDE analysis for hHMBSg1 and screening of HAP1 ΔHMBS clones	CAGAGGGTTAGTTCCTAGTA	Forward
	AGAGAGTGCAGTATCAAGAA	Reverse
Amplification of HMBS_232 from cDNA for cloning in pCMV-puroR	actctagaggatccgccaccATGTCTGGTAACGGCAATGC	Forward
	gtcctggttcgtgtggacctGTGATGGTGGTGATGATGATG	Reverse
Amplification of pCMV-puroR as backbone plasmid	GGTGGCGGATCCTCTAGAGT	Forward
	AGGTCCACACGAACCAGGAC	Reverse

794 **Table S8.** Sequences of primers. Lower-case letters indicate overhangs designed for
795 cloning with NEBuilder HiFi DNA Assembly Master Mix.
796
797 **Lentivirus production**
798 The following plasmids were used for lentivirus production: psPAX2 packaging plasmid
799 (Addgene, #12260), pMD2-G VSV-G envelope plasmid (Addgene, #12259), Blast-Cas9
800 plasmid, pKLV2-U6gRNA5(gGFP)-PGKBFP2AGFP-W reporter plasmid (Addgene,
801 #67980), and custom pooled CRISPR libraries. Lentiviruses were produced using the
802 following protocol. First, ~70% confluent HEK293FT cells in a 15 cm plate dish were
803 transfected with transfer, packaging, and envelope vectors in a 4:2:1 ratio. 125 µl of 2.5 M
804 calcium chloride was added to the plasmid mixture, and the final volume was made up to
805 1125 µl using 1 mM Tris, 0.1 mM EDTA, pH 8. The mixture was incubated at room
806 temperature for 5 min. Then 1250 µl of 2 x HBS (50 mM Hepes, 280 mM NaCl) was added
807 dropwise to the final plasmid solution while vortexing at full speed for 1 min. The mixture
808 was immediately added dropwise to HEK293FT cells. Approximately 16 h post-transfection,
809 the culture medium was replaced with fresh medium. The following day, ~30 h after media
810 replacement, cell supernatants were collected and filtered through a 0.45 µM filter to remove
811 cell debris. Virus-containing supernatants were ultracentrifuged for 2 h at 20,000 x g at 4 °C
812 (Hitachi CP100NX ultracentrifuge) and the pellet was aliquoted in 1 x PBS (~200 µl for
813 viruses produced from one 15 cm plate dish). Concentrated virus was aliquoted and stored
814 at -80 °C. Viruses were harvested every 24 h (by adding fresh medium to the HEK293FT
815 cells) for 3 - 4 days. The viral titer of concentrated viruses was calculated using the qPCR
816 Lentivirus Titration Kit from ABM (Applied Biological Materials, Vancouver, Canada)
817 according to the manufacturer's instructions.
818
819

820 **Generation of Cas9-expressing cell lines**

821 To achieve constitutive Cas9 expression, TaC12 and BoMac cell lines were infected with
822 lentiviruses containing the Cas9-Flag-Blast construct at a multiplicity of infection of 10.
823 Briefly, 100,000 – 500,000 cells were centrifuged at 100 x g for 5 min. The supernatant was
824 removed, and the cell pellet was resuspended in 1 ml medium containing 8 µg/ml of
825 polybrene. Aliquots of lentivirus stored at -80 °C were thawed on ice and the appropriate
826 volume of virions was added to the cells. Virus-cell solutions were incubated for 20 min at
827 room temperature, followed by a 30 min spin-infection performed at 30 °C in a laboratory
828 centrifuge (100 x g). After centrifugation, the pellet was resuspended in the same virus-
829 containing medium and cells were seeded into 6-well plates. After 24 h of incubation, the
830 supernatant was replaced with fresh medium containing blasticidin (Sigma-Aldrich, St. Louis
831 MO, USA) to select transduced cells (10 µg/ml for TaC12, 5 µg/ml for BoMac). For each cell
832 line, two controls were included in the experiment: positive control (non-transduced cells in
833 polybrene containing medium) and negative control (non-transduced cells in blasticidin
834 containing medium). When the negative controls reached 100% cell death, transduced
835 blasticidin-resistant cells were collected for validation of Cas9 expression by Western
836 blotting. A fluorescence-based reporter assay was performed to specifically select cells
837 expressing active Cas9. Briefly, Cas9-expressing cells were transduced with a lentiviral
838 vector consisting of blue fluorescent protein (BFP) and green fluorescent protein (GFP)
839 expression cassettes as indicated, together with a sgRNA targeting GFP. Cells were infected
840 at an MOI of 10 in the presence of 8 µg/ml of polybrene for 24 h and seeded into T25 flasks.
841 The culture medium was refreshed the following day. Between five and seven days after
842 transduction, cells were sorted by FACS for BFP+GFP- signal, indicating expression of
843 active Cas9 protein. For sorting, cells were resuspended in 1% FCS/PBS at a concentration
844 of 10 mio cells/ml. BFP+GFP- cells were collected in a Falcon tube containing 100% FCS,
845 centrifuged, and rapidly transferred to T25 flasks containing normal culture medium. Sorting

846 was repeated twice for enrichment, using the MoFlo ASTRIOS EQ cell sorter (Beckman
847 Coulter).
848
849 **CRISPR/Cas9 dropout screens**
850 Genome-wide CRISPR/Cas9 dropout screens were performed in Cas9-expressing TaC12
851 cells using a two-vector system, as well as small-scale screens in TaC12 and BoMac cells.
852 For the genome-scale screen we generated a CRISPR sgRNA containing 84,155 sgRNAs
853 targeting 21,039 protein-coding genes, with 4 sgRNAs designed per each gene. For the
854 small-scale screen we generated a CRISPR sgRNA library containing 16,596 sgRNAs
855 targeting 1,561 protein-coding genes, with 10 sgRNAs designed per each gene. Five
856 hundred non-targeting and 500 intergenic sgRNAs were added to each CRISPR library as
857 controls. The bovine libraries were cloned into lentiGuide-Puro plasmid (Addgene, #52963)
858 and viruses were produced in HEK293FT cells. Screens were performed at a coverage of
859 500 and in biological triplicates. A starting population of at least 140 mio cells (genome-wide
860 screen) or 60 mio cells (small-scale screen) was infected with the bovine lentiviral library in
861 normal growth medium in presence of polybrene (8 µg/ml) for 24 h. The next day, the culture
862 medium was replaced and fresh medium containing puromycin (2 µg/mL for TaC12; 1 µg/mL
863 for BoMac) was added to the cells. In both genome-wide and small-scale dropout screens,
864 a positive control (untransduced cells) and a negative control (untransduced cells treated
865 with puromycin) were included for each replicate of each CRISPR screen in all bovine cell
866 lines. After 3 days of puromycin selection the negative control reached complete cell death,
867 while successfully transduced cells were > 43 mio cells (e.g., 85,155 sgRNAs x 500) or > 9
868 mio cells (e.g., 17,596 sgRNAs x 500), corresponding to the previously calculated
869 transduction efficiency of ~30%. Puromycin-resistant cells were maintained in culture under
870 drug selection for at least 11 passages and harvested at the first and last passages for
871 genomic DNA (gDNA) extraction. gDNA was extracted from “START” and “END” point

872 samples and high-throughput Illumina sequencing was performed to quantify the abundance
873 of each sgRNA by PCR amplification of the sgRNA cassette. The resulting reads were
874 deconvoluted using the PoolQ tool
875 (https://portals.broadinstitute.org/gpp/public/software/poolq) to generate a matrix of read
876 counts, and transformed into log-norm files. Log2 fold change (LFC) values for each guide
877 were then generated by subtracting "END" point from "START" point values.
878
879 **Generation of HAP1 knockout cell line**
880 For human HMBS knockout, we chose a sgRNA targeting an early coding region of the
881 HMBS gene (5'-GCAGCTTGCTCGCATACAGA-3') and cloned this guide into the
882 pCRISPR_v3.1 plasmid. Low-passage HAP1 cells (< p5) were seeded at a concentration of
883 50,000 cells/well in 24 well plate. The following day, 600 ng of pCRISPR_v3.1+sgRNA
884 (HMBS) plasmid was transfected using Lipofectamine3000 according to manufacturer's
885 instructions. Twenty-four hours post transfection, the culture medium was refreshed and 0.6
886 µg/ml puromycin was added to the transfected cells as well as in the negative control.
887 Genomic DNA was extracted and the sgRNA (HMBS) target locus was PCR amplified using
888 Q5 High-Fidelity DNA polymerase (New England Biolabs, Ipswich, Massachusetts) (forward
889 primer: CAGAGGGTTAGTTCCTAGTA, reverse primer: AGAGAGTGCAGTATCAAGAA).
890 The resulting amplicon was purified using the Gel & PCR clean-up kit (Macherey-Nagel,
891 Düren, Germany) and sequenced by Sanger sequencing. The online tool Tracking of Indels
892 by Decomposition (TIDE) was used to interpret the sequencing results. Limiting dilutions of
893 the polyclonal HAP1 ΔHMBS pool were performed in 96 well plate, and six isolated clones
894 were selected. Successful knockout of the HMBS gene was verified at genome level
895 (identification of frameshift mutations at the target locus) and at the protein expression level
896 (Western blotting).
897

898 **Re-expression of HMBS in HAP1 ΔHMBS clone A**

899 The housekeeping isoform of HMBS transcript (ENST00000652429.1, HMBS_232) was
900 amplified from complementary DNA synthesized by reverse transcriptase starting from RNA
901 of HAP1 WT cells (GoScript™ Reverse Transcriptase, Promega, Madison WI, USA).
902 HMBS_232 was cloned into pCMV-puroR lentiviral plasmid using the primers listed in Table
903 S6 and NEBuilder HiFi DNA Assembly Master Mix (New England BioLabs). Lentiviruses
904 were produced as already mentioned. HAP1 ΔHMBS cells were transduced for 24h with
905 virus-containing supernatants harvested from HEK293FT dishes, and cells were selected
906 for 4 days with 0.6 µg/ml puromycin. Untransduced HAP1 ΔHMBS cells were used as a
907 negative control and reached 100% cell death following 4 days of puromycin selection.
908 Puromycin-resistant cells were subjected to limiting dilutions, and several single clones were
909 analyzed via Western blotting for HMBS expression.

910

911 **Western blotting**

912 Whole cell lysates were prepared by lysing 5 mio cells in 500 µl lysis buffer (50 mM Tris-
913 HCl, 150 mM NaCl, 1 mM EDTA, 1% NP-40, 0.25% sodium deoxycholate, 1x cOmplete™
914 protease inhibitor cocktail (Roche, Basel, Switzerland). The samples were boiled for 5 min
915 at 90 °C, and then cooled on ice. Whole cell lysates were then loaded onto 10% sodium
916 dodecyl sulphate (SDS) polyacrylamide gels. Gel runs lasted 45 - 50 min at 25 mA in
917 electrophoresis buffer (2.5 mM Tris, 19.2 mM glycine, 0.01% SDS), followed by protein
918 transfer to a nitrocellulose membrane for 90 min at 400 mA in transfer buffer (20 mM Tris-
919 HCl, 15 mM glycine, 20% (v/v) methanol). The membrane was incubated for several hours
920 in blocking solution (5% milk powder in TBST (10 mM Tris, 150 mM NaCl, 0.05% Tween).
921 Primary antibodies were diluted in blocking solution and incubated with the membrane
922 overnight at 4 °C. After three washes with TBS (10 mM Tris, 150 mM NaCl), the membrane
923 was incubated with secondary antibodies diluted in blocking solution for 45 min at room

924 temperature. If fluorescent secondary antibodies were used, incubation was performed in
925 the dark. After three further washes with TBS, the Western blot was then imaged using the
926 C600 imaging system (Azure Biosystems).
927
928 **FCS heme depletion**
929 Heme-depleted FCS was prepared by treating FCS with 20 mM ascorbic acid for 16 h at 37
930 °C, followed by 24 h dialysis against PBS. Heme depletion was verified by measuring optical
931 absorbance at 405 nm.[65]
932
933 **Cell viability assay**
934 Cell viability assays were performed in 96 well plates. Briefly, 5,000 TaC12 or BoMac cells
935 were seeded into the 96 wells and cells were allowed to grow for 72 h under normal culture
936 conditions in the presence of inhibitors or solvent alone. Cell viability was measured using
937 the resazurin assay.
938
939 **Mouse experiments and mosquito maintenance**
940 Mouse studies were approved by the Commission for Animal Experimentation of the
941 Cantonal Veterinary Office of Bern and conducted in compliance with the Swiss Animal
942 Welfare legislation and under license BE118/22. Mice were infected by i.p. injection of blood
943 stabilates of mCherry expressing *Plasmodium berghei* parasites (RMgm-928, 1804cl1). At
944 approximately 4% parasitemia, blood was collected by cardiac puncture and passaged by
945 i.v. injection into a new mouse (feed mouse). After 3 days, the parasitemia and
946 gametocytemia were monitored by flow cytometry (NovoCyte, Agilent) and thin blood smear.
947 At >0.4% gametocytes, the mice were anaesthetized (ketamin/xylazine) and made available
948 to approximately 150 female *Anopheles stephensi* mosquitoes to take a blood meal for 30
949 min. The mosquitoes were maintained at 20.5 °C and above 80% relative humidity.

950 Sporozoites were isolated from infected salivary glands on days 18 - 26 after the infective
951 blood meal.
952
953 ***Plasmodium berghei* infection**
954 HAP1 cells were cultured in IMDM (Bioconcept, containing 10% FCS, 4 mM L-glutamine,
955 100 U penicillin, 100 µg/ml streptomycin) at 37° C, 5% CO_2. To infect confluent cultures,
956 70,000 cells were seeded in 96 well plates. The next day, the cultures were infected with
957 20,000 freshly isolated sporozoites. To allow development over 48 h, cultures were
958 expanded by passaging with accutase (Innovative Cell Technologies) at 2 hpi. Cells were
959 reseeded into 96 well plates (Greiner µClear, 655090). Each infected well was divided into
960 12 wells. At 48 hpi, cells were imaged with a Nikon Ti2 inverted fluorescence microscope
961 (Plan Apo λD 10× (NA 0.45) objective, Spectra X light engine (555nm line, Lumencor),
962 acquired with a Kinetix22 camera (Photometrix), Pinkel quad and Sedat quad filter sets
963 (MXR00244 and MXR00254, Semrock). Parasite sizes were segmented and analyzed using
964 the General Analysis Module of NIS-Elements 5.42.02. Graphs were generated with Prism
965 9 (GraphPad).
966

967 **SUPPLEMENTAL INFORMATION**

968

H2O	D-Fructose	L-1-Pyrroline-3-hydroxy-5-carboxylate	Orthophosphate
(9Z)-Octadecenoic acid	D-Glucosamine	L-2-Amino-3-oxobutanoic acid	Oxaloacetate
(R)-Lactate	D-Glucose	L-Alanine	Oxygen
(R)-S-Lactoylglutathione	D-Glyceraldehyde	L-Arginine	Pantetheine
(S)-1-Pyrroline-5-carboxylate	D-Mannose	L-Asparagine	Pantothenate
(S)-Dihydroorotate	Deoxyadenosine	L-Aspartate	Phenylpyruvate
(S)-Lactate	Deoxycytidine	L-Cysteate	Propanoate
(S)-Malate	Deoxyguanosine	L-Cysteine	Protein asparagine
1,2-Diacyl-sn-glycerol	Deoxyinosine	L-Glutamate	Protoporphyrinogen IX
10-Formyltetrahydrofolate	Deoxyuridine	L-Glutamate 5-semialdehyde	Pyridoxal
2-Oxobutanoate	Dihydroceramide	L-Glutamine	Pyridoxamine
2-Oxoglutarate	Dihydrofolate	L-Histidine	Pyridoxine
3-(4-Hydroxyphenyl)pyruvate	Diphosphate	L-Homocysteine	Pyruvate
3-Dehydrosphinganine	DL-Glutamate	L-Isoleucine	Retinal
3-Mercaptolactate	Dodecanoic acid	L-Leucine	Retinol
3-Sulfino-L-alanine	Ethanolamine	L-Lysine	Riboflavin
3-Sulfopyruvate	Fe2+	L-Methionine	S-Adenosyl-L-homocysteine
4-Aminobutanoate	Ferricytochrome b5	L-Ornithine	S-Adenosyl-L-methionine
4-Hydroxybenzoate	Ferrocytochrome b5	L-Phenylalanine	S-Adenosylmethioninamine
5-MethylTHF	Folate	L-Proline	Spermine
5-Methylthioadenosine	Formaldehyde	L-Selenomethionine	Sphinganine
5,10-MethenylTHF	Formate	L-Serine	Sphingosine
5,10-MethyleneTHF	Fumarate	L-Threonine	Succinate
6-Pyruvoyltetrahydropterin	gamma-L-Glutamyl-L-cysteine	L-Tryptophan	Sulfate
9-cis-Retinol	Glutathione	L-Tyrosine	Sulfite

Acetaldehyde	Glutathione disulfide	L-Valine	Sulfur donor
Acetate	Glycerol	Linoleate	Tetradecanoic acid
Adenine	Glycerone	Lipoate	THF
Adenosine	Glycine	Mercaptopyruvate	Thiamine
Apoprotein	Glycolaldehyde	Methanol	Thioredoxin
Arachidonate	Glyoxylate	Methylcobalamin	Thioredoxin disulfide
Benzoate	Guanine	myo-Inositol	trans-4-Hydroxy-L-proline
Biotin	Guanosine	N-Acylsphingosine	Triacylglycerol
Cholesterol	H_passed_ETC	N-Carbamoyl-L-aspartate	Triphosphate
Choline	H+	N-Ribosylnicotinamide	Uracil
cis-Aconitate	HCO3-	NH3	Urea
Citrate	Heme	Nicotinamide	Uridine
CO2	Hexadecanoic acid	Nicotinate	Xanthine
Coproporphyrinogen III	Hydrogen peroxide	Nicotinate D-ribonucleoside	Xanthosine
Cys-Gly	Hypoxanthine	Nitrite	
Cytidine	Inosine	Octadecanoic acid	
D-4-Hydroxy-2-oxoglutarate	Isocitrate	Orotate	

Table S1. Composition of rich extra-parasitic environment. 165 compounds that are available in the cytosol of the human Recon 3D model and that are part of the extracellular environment of the *Plasmodium falciparum* iPfa model. THF: tetrahydrofolate.

Table S2. Hypergeometric analysis of bovine genome-wide CRISPR screen in TaC12 cells. Average LFC values of the three screening replicates (Average_LFC) were normalized using the dispersion of intergenic and non-target controls (z-norm LFC).

Table S3. Hypergeometric analysis of bovine small-scale CRISPR screen in TaC12 cells. Average LFC values of the three screening replicates (i_Average_LFC; u_Average_LFC) were normalized using the dispersion of intergenic and non-target controls (i_z_LFC; u_z_LFC).

982

983 **Table S4. Fitness-scoring genes in small-scale CRISPR screen in TaC12 cells and**
984 **dispensable for BoMac (*Theileria essentialome*)**. Average LFC values of the three
985 screening replicates (i_Average_LFC; u_Average_LFC) were normalized using the
986 dispersion of intergenic and non-target controls (i_z_LFC; u_z_LFC).

987

988 **Table S5. Gene Ontology analysis of *Theileria essentialome* (ShinyGO v.066).**

989

990 **Figure S1. Computational analysis of *P. falciparum* nutritional requirements and**
991 **dependence on hepatocyte genes, related to Figure 2. (A)** Scheme of the computational
992 workflow to generate *parasitosomes*: 1. Define the extra-parasitic environment; 2. Identify
993 the reactions required for growth under the given conditions, and alternatives; 3. Extract the
994 corresponding *parasitosome* reactions by collapsing the reactions identified in step 2 into
995 one reaction containing the nutrients and products that each parasite state takes up and
996 secretes into the host cytosol. **(B)** Composition of the compromised extra-parasitic
997 environment, where the parasite has access to only the minimum set of metabolites (47
998 metabolites) required for growth. Participation in the alternative iMM sets determines
999 whether each metabolite is constitutive, if it is required in all the alternatives, or substitutable,
1000 if another metabolite can substitute its function. **(C)** Metabolic subsystems composing the
1001 different networks for the *parasitosomes*, when considering a rich (green) or a compromised
1002 (orange) extra-parasitic environment (ePE), in terms of number of reactions and percentage
1003 of subsystem coverage. **(D)** Metabolic composition of the alternative *parasitosomes* in case
1004 study I (rich ePE, green) and II (compromised ePE, orange). The frequency indicates
1005 whether the nutrients and products are constitutive if they appear in all alternative
1006 *parasitosomes*.

1007

1008 **Figure S2. Computational analysis of *P. falciparum* nutritional requirements and**
1009 **dependence on hepatocyte genes, related to Figure 2.** Complete list of metabolic
1010 subsystems associated with hepatocyte genes that are essential for at least one
1011 *parasitosome*. Classification of the genes based on their frequency of essentiality across
1012 *parasitosomes*, the number of essential genes associated with each subsystem and the
1013 percentage of essential genes out of the total genes associated with each subsystem in
1014 case study I (rich ePE, green) and case study II (compromised ePE, orange).
1015
1016 **Figure S3. Hepatocyte genes essential for *P. falciparum* and dispensable for the host,**
1017 **related to Figure 2.** (**A**) List of genes essential in the healthy hepatocyte model. (**B - C**)
1018 Classification of genes per metabolic pathway and the frequency of their essentiality across
1019 *parasitosomes* in case study I (rich ePE, green) and in case study II (compromised ePE,
1020 orange). Genes essential for all *parasitosomes* are highlighted in red. (**D**) List of 19 genes
1021 essential for all *parasitosomes.*
1022
1023 **Figure S4. Cas9-expression in *Theileria*-infected macrophages and supplementary**
1024 **data on genetic screens, related to Figure 3. (A)** Western blot of whole cell lysates from
1025 Cas9-TaC12 and TaC12 WT. Flag-tagged Cas9 is expressed in TaC12 cells after
1026 transduction with Cas9-Flag-Blast lentiviruses. Tubulin staining served as a loading control.
1027 **(B)** Schematic representation of the lentiviral vector used for Cas9 activity assay. In
1028 transduced cells with no active Cas9 protein, both GFP and BFP fluorescence are
1029 detectable. When Cas9 is active, the GFP sequence gets cleaved and only the BFP
1030 fluorescence is detected. CMV, CMV promoter; RU5, 5' long terminal repeat; hU6, human
1031 U6 promoter; gGFP, sgRNA targeting GFP gene; PGK, mouse *Pgk1* promoter; BFP, blue
1032 fluorescent protein gene; 2A, *Thosea asigna* virus 2A peptides; GFP, green fluorescent
1033 protein gene; W, Woodchuck hepatitis virus posttranscriptional regulatory element;

1034 ΔU3RU5, self-inactivating 3' LTR. **(C)** TaC12-Cas9 expressing cells were analyzed by
1035 fluorescence-activated cell sorting (FACS) prior to cell sorting for BFP+/GFP- signal. The
1036 cell population expressing an active Cas9 protein (BFP+/GFP-) was sorted twice to enrich
1037 for BFP-positive cells. The BFP-positive gate was strictly set to enrich for the brightest
1038 fluorescing cells. Most cells transduced with the reporter construct are BFP+/GFP- while a
1039 small fraction is BFP/GFP double positive, indicating the absence of active Cas9. The same
1040 procedure was performed with BoMac-Cas9 cells. **(D)** Principal component analysis plot of
1041 log-norm count distribution of the TaC12 genome-wide screens. DAY0 and END points for
1042 each biological replicate are shown, as well as the distribution of the CRISPR library
1043 (log.library). **(E)** Library representation at DAY0 and END points of TaC12 genome-wide
1044 screen replicates. **(F)** Volcano plot showing the hypergeometric distribution analysis of the
1045 CRISPR/Cas9 small-scale screen in TaC12. Each gene is plotted based on its average LFC
1046 (z-normalized using the control dispersion) and the negative $\log_{10}$ of its *p*-value. A selected
1047 set of 100 genes that were found to be non-essential in TaC12_GW is shown in orange. A
1048 group of ~ 800 genes significantly depleted in TaC12_GW (orig_TAC) is shown in yellow.
1049 The vertical dotted line corresponds to the average z-normalized LFC of the controls
1050 (intergenic and non-targeting) minus 1x standard deviation of the entire genetic screen. The
1051 screen was performed in 3 biological replicates. **(G)** Library representation at DAY0 and
1052 END points of TaC12 small scale screen replicates. **(H)** Volcano plot showing the
1053 hypergeometric distribution analysis of the CRISPR/Cas9 small-scale screen in BoMac.
1054 Each gene is plotted based on its average LFC (z-normalized using the control dispersion)
1055 and the negative $\log_{10}$ of its p-value. A selected set of 100 genes that were found to be non-
1056 essential in TaC12_GW is shown in orange. A group of ~ 800 genes significantly depleted
1057 in TaC12_GW (orig_TAC) is shown in yellow. The vertical dotted line corresponds to the
1058 average z-normalized LFC of the controls (intergenic and non-targeting) minus 1x standard

1059 deviation of the entire genetic screen. The screen was performed in 3 biological replicates.
1060 **(I)** Library representation at DAY0 and END points of BoMac small scale screen replicates.
1061
1062 **Figure S5. TCA cycle genes are enriched in the *Theileria essentialome*, related to**
1063 **Figure 4. (A)** Representation of the TCA cycle by KEGG. Fitness-conferring genes in TaC12
1064 are shown in red. **(B)** Scoring of genes belonging to the TCA cycle in TaC12 vs BoMac
1065 screens.
1066
1067 **Figure S6. Purine metabolism genes are enriched in the *Theileria essentialome*,**
1068 **related to Figure 4. (A)** Representation of purine metabolism by KEGG. Fitness-conferring
1069 genes in TaC12 are shown in red. **(B)** Scoring of genes belonging to the TCA cycle in TaC12
1070 vs BoMac screens.
1071
1072 **Figure S7. Supplementary data related to Figure 5. (A)** TIDE analysis of *GSS*, *SRM* and
1073 *HMBS* CRISPR/Cas9 knockouts in TaC12 and BoMac cells. **(B)** TIDE analysis of vimentin
1074 (*VIM*) CRISPR/Cas9 knockout in TaC12 and BoMac cells. Vimentin is a non-essential gene
1075 in many cell lines, and we use it as a positive control that it can be knocked out in TaC12
1076 and BoMac cells. **(C-E)** Resazurin viability assays showing the percentage of survival of
1077 BoMac and TaC12 cells after 72 hours treatment with buthionine sulfoximine (BSO), sodium
1078 nitroprusside (SNP), salicylic acid (SA). **(F)** Western blot of whole cell lysates from HAP1
1079 WT and HAP1 ΔHMBS clones A-B-C-D-E-F. Tubulin staining served as loading control.
1080

1081 **REFERENCES**

1082

1083 1. Adl SM, Leander BS, Simpson AG, Archibald JM, Anderson OR, Bass D, et al.
1084 Diversity, nomenclature, and taxonomy of protists. Syst Biol. 2007;56(4):684-9.

1085

1086 2. WHO. WHO World Malaria Report 2021.

1087

1088 3. Morrison WI. The aetiology, pathogenesis and control of theileriosis in domestic
1089 animals. Rev Sci Tech. 2015;34(2):599-611.

1090

1091 4. Nene V, Kiara H, Lacasta A, Pelle R, Svitek N, Steinaa L. The biology of *Theileria*
1092 *parva* and control of East Coast fever - Current status and future trends. Ticks Tick Borne
1093 Dis. 2016;7(4):549-64.

1094

1095 5. Agina OA, Shaari MR, Isa NMM, Ajat M, Zamri-Saad M, Hamzah H. Clinical
1096 pathology, immunopathology and advanced vaccine technology in bovine theileriosis: A
1097 review. Pathogens. 2020;9(9).

1098

1099 6. Liu J, Guan G, Yin H. Theileria annulata. Trends Parasitol. 2022;38(3):265-6.

1100

1101 7. Dobbelaere DA, Rottenberg S. *Theileria*-induced leukocyte transformation. Curr Opin
1102 Microbiol. 2003;6(4):377-82.

1103

1104 8. Tretina K, Gotia HT, Mann DJ, Silva JC. Theileria-transformed bovine leukocytes
1105 have cancer hallmarks. Trends Parasitol. 2015;31(7):306-14.

1106 9. Guerin A, Striepen B. The biology of the intestinal intracellular parasite
1107 *Cryptosporidium*. Cell Host Microbe. 2020;28(4):509-15.
1108
1109 10. Krishnan A, Kloehn J, Lunghi M, Chiappino-Pepe A, Waldman BS, Nicolas D, et al.
1110 Functional and computational genomics reveal unprecedented flexibility in stage-specific
1111 *Toxoplasma* metabolism. Cell Host Microbe. 2020;27(2):290-306 e11.
1112
1113 11. Olszewski KL, Morrisey JM, Wilinski D, Burns JM, Vaidya AB, Rabinowitz JD, et al.
1114 Host-parasite interactions revealed by *Plasmodium falciparum* metabolomics. Cell Host
1115 Microbe. 2009;5(2):191-9.
1116
1117 12. Wang T, Wei JJ, Sabatini DM, Lander ES. Genetic screens in human cells using the
1118 CRISPR-Cas9 system. Science. 2014;343(6166):80-4.
1119
1120 13. Todor H, Silvis MR, Osadnik H, Gross CA. Bacterial CRISPR screens for gene
1121 function. Curr Opin Microbiol. 2021;59:102-9.
1122
1123 14. Wagner JC, Platt RJ, Goldfless SJ, Zhang F, Niles JC. Efficient CRISPR-Cas9-
1124 mediated genome editing in *Plasmodium falciparum*. Nat Methods. 2014;11(9):915-8.
1125
1126 15. Sidik SM, Huet D, Ganesan SM, Huynh MH, Wang T, Nasamu AS, et al. A genome-
1127 wide CRISPR screen in *Toxoplasma* identifies essential apicomplexan genes. Cell.
1128 2016;166(6):1423-35 e12.
1129

1130 16. Stanway RR, Bushell E, Chiappino-Pepe A, Roques M, Sanderson T, Franke-Fayard
1131 B, et al. Genome-scale identification of essential metabolic processes for targeting the
1132 *Plasmodium* liver stage. Cell. 2019;179(5):1112-28 e26.
1133
1134 17. Vijayan K, Arang N, Wei L, Morrison R, Geiger R, Parks KR, et al. A genome-wide
1135 CRISPR-Cas9 screen identifies CENPJ as a host regulator of altered microtubule
1136 organization during *Plasmodium* liver infection. Cell Chem Biol. 2022;29(9):1419-33 e5.
1137
1138 18. Wu SZ, Wei HX, Jiang D, Li SM, Zou WH, Peng HJ. Genome-wide CRISPR screen
1139 identifies host factors required by *Toxoplasma gondii* infection. Front Cell Infect Microbiol.
1140 2019;9:460.
1141
1142 19. Gibson AR, Sateriale A, Dumaine JE, Engiles JB, Pardy RD, Gullicksrud JA, et al. A
1143 genetic screen identifies a protective type III interferon response to *Cryptosporidium* that
1144 requires TLR3 dependent recognition. PLoS Pathog. 2022;18(5):e1010003.
1145
1146 20. Thiele I, Palsson BO. A protocol for generating a high-quality genome-scale metabolic
1147 reconstruction. Nat Protoc. 2010;5(1):93-121.
1148
1149 21. Sen P, Oresic M. Integrating omics data in genome-scale metabolic modeling: A
1150 methodological perspective for precision medicine. Metabolites. 2023;13(7).
1151
1152 22. Plata G, Hsiao TL, Olszewski KL, Llinas M, Vitkup D. Reconstruction and flux-balance
1153 analysis of the *Plasmodium falciparum* metabolic network. Mol Syst Biol. 2010;6:408.
1154

1155 23. Bazzani S, Hoppe A, Holzhutter HG. Network-based assessment of the selectivity of
1156 metabolic drug targets in *Plasmodium falciparum* with respect to human liver metabolism.
1157 BMC Syst Biol. 2012;6:118.
1158
1159 24. Huthmacher C, Hoppe A, Bulik S, Holzhutter HG. Antimalarial drug targets in
1160 *Plasmodium falciparum* predicted by stage-specific metabolic network analysis. BMC Syst
1161 Biol. 2010;4:120.
1162
1163 25. Chiappino-Pepe A, Tymoshenko S, Ataman M, Soldati-Favre D, Hatzimanikatis V.
1164 Bioenergetics-based modeling of *Plasmodium falciparum* metabolism reveals its essential
1165 genes, nutritional requirements, and thermodynamic bottlenecks. PLoS Comput Biol.
1166 2017;13(3):e1005397.
1167
1168 26. O'Brien EJ, Monk JM, Palsson BO. Using genome-scale models to predict biological
1169 capabilities. Cell. 2015;161(5):971-87.
1170
1171 27. Richelle A, Kellman BP, Wenzel AT, Chiang AWT, Reagan T, Gutierrez JM, et al.
1172 Model-based assessment of mammalian cell metabolic functionalities using omics data. Cell
1173 Rep Methods. 2021;1(3).
1174
1175 28. Karlsson M, Zhang C, Mear L, Zhong W, Digre A, Katona B, et al. A single-cell type
1176 transcriptomics map of human tissues. Sci Adv. 2021;7(31).
1177
1178 29. Mardinoglu A, Agren R, Kampf C, Asplund A, Uhlen M, Nielsen J. Genome-scale
1179 metabolic modelling of hepatocytes reveals serine deficiency in patients with non-alcoholic
1180 fatty liver disease. Nat Commun. 2014;5:3083.

1181

1182 30. Gille C, Bolling C, Hoppe A, Bulik S, Hoffmann S, Hubner K, et al. HepatoNet1: a
1183 comprehensive metabolic reconstruction of the human hepatocyte for the analysis of liver
1184 physiology. Mol Syst Biol. 2010;6:411.

1185

1186 31. Masid M, Ataman M, Hatzimanikatis V. Analysis of human metabolism by reducing
1187 the complexity of the genome-scale models using redHUMAN. Nat Commun.
1188 2020;11(1):2821.

1189

1190 32. Brunk E, Sahoo S, Zielinski DC, Altunkaya A, Drager A, Mih N, et al. Recon3D
1191 enables a three-dimensional view of gene variation in human metabolism. Nat Biotechnol.
1192 2018;36(3):272-81.

1193

1194 33. Wei L, Adderley J, Leroy D, Drewry DH, Wilson DW, Kaushansky A, et al. Host-
1195 directed therapy, an untapped opportunity for antimalarial intervention. Cell Rep Med.
1196 2021;2(10):100423.

1197

1198 34. Vijayan K, Wei L, Glennon EKK, Mattocks C, Bourgeois N, Staker B, et al. Host-
1199 targeted interventions as an exciting opportunity to combat malaria. Chem Rev.
1200 2021;121(17):10452-68.

1201

1202 35. Garrido-Cardenas JA, Cebrian-Carmona J, Gonzalez-Ceron L, Manzano-Agugliaro
1203 F, Mesa-Valle C. Analysis of global research on malaria and *Plasmodium vivax*. Int J Environ
1204 Res Public Health. 2019;16(11).

1205

1206 36. Hart T, Brown KR, Sircoulomb F, Rottapel R, Moffat J. Measuring error rates in
1207 genomic perturbation screens: gold standards for human functional genomics. Mol Syst Biol.
1208 2014;10(7):733.
1209
1210 37. Griffith OW, Meister A. Potent and specific inhibition of glutathione synthesis by
1211 buthionine sulfoximine (S-n-butyl homocysteine sulfoximine). J Biol Chem.
1212 1979;254(16):7558-60.
1213
1214 38. Bauer PM, Buga GM, Fukuto JM, Pegg AE, Ignarro LJ. Nitric oxide inhibits ornithine
1215 decarboxylase via S-nitrosylation of cysteine 360 in the active site of the enzyme. J Biol
1216 Chem. 2001;276(37):34458-64.
1217
1218 39. Gupta V, Liu S, Ando H, Ishii R, Tateno S, Kaneko Y, et al. Salicylic acid induces
1219 mitochondrial injury by inhibiting ferrochelatase heme biosynthesis activity. Mol Pharmacol.
1220 2013;84(6):824-33.
1221
1222 40. Fox BA, Bzik DJ. Biochemistry and metabolism of *Toxoplasma gondii*: purine and
1223 pyrimidine acquisition in *Toxoplasma gondii* and other Apicomplexa. In: *Toxoplasma gondii*
1224 The model apicomplexan. Perspectives and methods. 2020:54.
1225
1226 41. Kloehn J, Harding CR, Soldati-Favre D. Supply and demand-heme synthesis,
1227 salvage and utilization by Apicomplexa. FEBS J. 2021;288(2):382-404.
1228
1229 42. Caldelari R, Dogga S, Schmid MW, Franke-Fayard B, Janse CJ, Soldati-Favre D, et
1230 al. Transcriptome analysis of *Plasmodium berghei* during exo-erythrocytic development.
1231 Malar J. 2019;18(1):330.

1232

1233 43. Rathnapala UL, Goodman CD, McFadden GI. A novel genetic technique in
1234 *Plasmodium berghei* allows liver stage analysis of genes required for mosquito stage
1235 development and demonstrates that de novo heme synthesis is essential for liver stage
1236 development in the malaria parasite. PLoS Pathog. 2017;13(6):e1006396.

1237

1238 44. Wagner BA, Teesch LM, Buettner GR, Britigan BE, Burns CP, Reszka KJ. Inactivation
1239 of anthracyclines by serum heme proteins. Chem Res Toxicol. 2007;20(6):920-6.

1240

1241 45. Krishnan A, Soldati-Favre D. Amino acid metabolism in Apicomplexan parasites.
1242 Metabolites. 2021;11(2).

1243

1244 46. Dobbelaere D, Heussler V. Transformation of leukocytes by *Theileria parva* and *T.*
1245 *annulata*. Annu Rev Microbiol. 1999;53:1-42.

1246

1247 47. Tellez J, Romero I, Soares MJ, Steindel M, Romanha AJ. Knockdown of host
1248 antioxidant defense genes enhances the effect of glucantime on intracellular *Leishmania*
1249 *braziliensis* in human macrophages. Antimicrob Agents Chemother. 2017;61(7).

1250

1251 48. Niu B, Liao K, Zhou Y, Wen T, Quan G, Pan X, et al. Application of glutathione
1252 depletion in cancer therapy: Enhanced ROS-based therapy, ferroptosis, and chemotherapy.
1253 Biomaterials. 2021;277:121110.

1254

1255 49. Zhang Y, Tan H, Daniels JD, Zandkarimi F, Liu H, Brown LM, et al. Imidazole ketone
1256 erastin induces ferroptosis and slows tumor growth in a mouse lymphoma model. Cell Chem
1257 Biol. 2019;26(5):623-33 e9.

1258

1259 50. Cruz A, Mota P, Ramos C, Pires RF, Mendes C, Silva JP, et al. Polyurea dendrimer
1260 folate-targeted nanodelivery of l-buthionine sulfoximine as a tool to tackle ovarian cancer
1261 chemoresistance. Antioxidants. 2020;9(2).

1262

1263 51. Cook T, Roos D, Morada M, Zhu G, Keithly JS, Feagin JE, et al. Divergent polyamine
1264 metabolism in the Apicomplexa. Microbiology. 2007;153(Pt 4):1123-30.

1265

1266 52. Birkholtz LM, Williams M, Niemand J, Louw AI, Persson L, Heby O. Polyamine
1267 homoeostasis as a drug target in pathogenic protozoa: peculiarities and possibilities.
1268 Biochem J. 2011;438(2):229-44.

1269

1270 53. Phillips MA. Polyamines in protozoan pathogens. J Biol Chem. 2018;293(48):18746-
1271 56.

1272

1273 54. Haider N, Eschbach ML, Dias Sde S, Gilberger TW, Walter RD, Luersen K. The
1274 spermidine synthase of the malaria parasite *Plasmodium falciparum*: molecular and
1275 biochemical characterisation of the polyamine synthesis enzyme. Mol Biochem Parasitol.
1276 2005;142(2):224-36.

1277

1278 55. Rizopoulos Z, Matuschewski K, Haussig JM. Distinct prominent roles for enzymes of
1279 *Plasmodium berghei* heme biosynthesis in sporozoite and liver stage maturation. Infect
1280 Immun. 2016;84(11):3252-62.

1281

1282 56. Nagaraj VA, Sundaram B, Varadarajan NM, Subramani PA, Kalappa DM, Ghosh SK,
1283 et al. Malaria parasite-synthesized heme is essential in the mosquito and liver stages and

1284 complements host heme in the blood stages of infection. PLoS Pathog.
1285 2013;9(8):e1003522.
1286
1287 57. Ke H, Sigala PA, Miura K, Morrisey JM, Mather MW, Crowley JR, et al. The heme
1288 biosynthesis pathway is essential for *Plasmodium falciparum* development in mosquito
1289 stage but not in blood stages. J Biol Chem. 2014;289(50):34827-37.
1290
1291 58. Sigala PA, Crowley JR, Henderson JP, Goldberg DE. Deconvoluting heme
1292 biosynthesis to target blood-stage malaria parasites. Elife. 2015;4.
1293
1294 59. Tweedell RE, Tao D, Hamerly T, Robinson TM, Larsen S, Gronning AGB, et al. The
1295 selection of a hepatocyte cell line susceptible to *Plasmodium falciparum* sporozoite invasion
1296 that is associated with expression of glypican-3. Front Microbiol. 2019;10:127.
1297
1298 60. Kilburn DG, Lilly MD, Webb FC. The energetics of mammalian cell growth. J Cell Sci.
1299 1969;4(3):645-54.
1300
1301 61. Ataman M, Hatzimanikatis V. lumpGEM: Systematic generation of subnetworks and
1302 elementally balanced lumped reactions for the biosynthesis of target metabolites. PLoS
1303 Comput Biol. 2017;13(7):e1005513.
1304
1305 62. Noedl H, Se Y, Schaecher K, Smith BL, Socheat D, Fukuda MM, et al. Evidence of
1306 artemisinin-resistant malaria in western Cambodia. N Engl J Med. 2008;359(24):2619-20.
1307

1308 63. Becker SA, Feist AM, Mo ML, Hannum G, Palsson BO, Herrgard MJ. Quantitative
1309 prediction of cellular metabolism with constraint-based models: the COBRA Toolbox. Nat
1310 Protoc. 2007;2(3):727-38.
1311
1312 64. Stabel JR, Stabel TJ. Immortalization and characterization of bovine peritoneal
1313 macrophages transfected with SV40 plasmid DNA. Vet Immunol Immunopathol. 1995;45(3-
1314 4):211-20.
1315
1316 65. Galmozzi A, Kok BP, Kim AS, Montenegro-Burke JR, Lee JY, Spreafico R, et al.
1317 PGRMC2 is an intracellular haem chaperone critical for adipocyte function. Nature.
1318 2019;576(7785):138-42.
1319

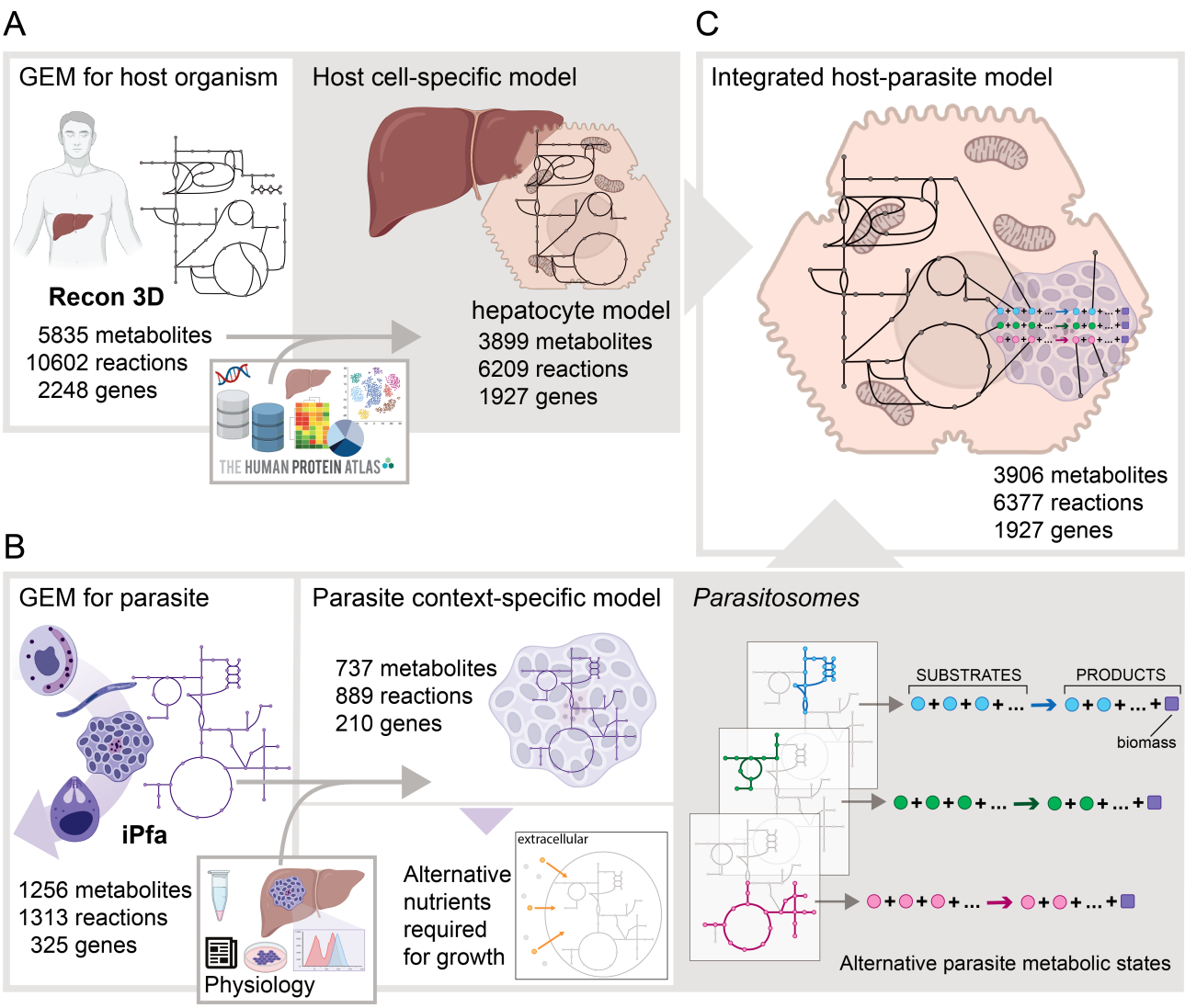

1320

1321 **Figure 1**

1322

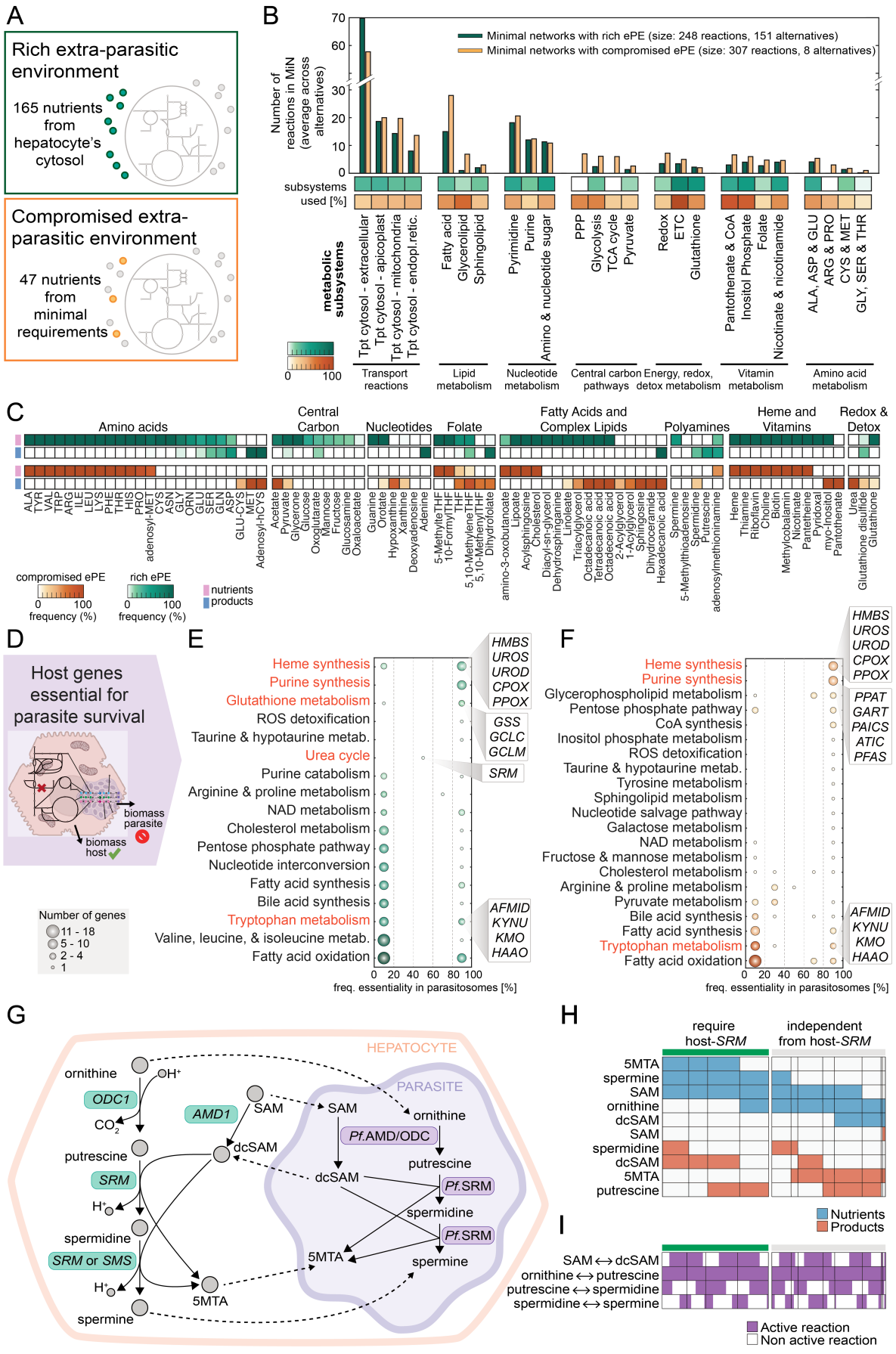
A
Rich extra-parasitic environment
165 nutrients from hepatocyte's cytosol
Compromised extra-parasitic environment
47 nutrients from minimal requirements
B
Minimal networks with rich ePE (size: 248 reactions, 151 alternatives)
Minimal networks with compromised ePE (size: 307 reactions, 8 alternatives)
Number of reactions in MiN (average across alternatives)
subsystems used [%]
metabolic subsystems
Tpt cytosol - extracellular
Tpt cytosol - apicoplast
Tpt cytosol - mitochondria
Tpt cytosol - endopl.retic.
Fatty acid
Glycerolipid
Sphingolipid
Pyrimidine
Purine
Amino & nucleotide sugar
PPP
Glycolysis
TCA cycle
Pyruvate
Redox
ETC
Glutathione
Pantothenate & CoA
Inositol Phosphate
Folate
Nicotinate & nicotinamide
ALA, ASP & GLU
ARG & PRO
CYS & MET
GLY, SER & THR
Transport reactions
Lipid metabolism
Nucleotide metabolism
Central carbon pathways
Energy, redox, detox metabolism
Vitamin metabolism
Amino acid metabolism
C
Amino acids
Central Carbon
Nucleotides
Folate
Fatty Acids and Complex Lipids
Polyamines
Heme and Vitamins
Redox & Detox
compromised ePE
rich ePE
frequency (%)
nutrients
products
D
Host genes essential for parasite survival
biomass parasite
biomass host
Number of genes
11 - 18
5 - 10
2 - 4
1
E
Heme synthesis
Purine synthesis
Glutathione metabolism
ROS detoxification
Taurine & hypotaurine metab.
Urea cycle
Purine catabolism
Arginine & proline metabolism
NAD metabolism
Cholesterol metabolism
Pentose phosphate pathway
Nucleotide interconversion
Fatty acid synthesis
Bile acid synthesis
Tryptophan metabolism
Valine, leucine, & isoleucine metab.
Fatty acid oxidation
HMBS
UROS
UROD
CPOX
PPOX
GSS
GCLC
GCLM
SRM
AFMID
KYNU
KMO
HAAO
freq. essentiality in parasitosomes [%]
F
Heme synthesis
Purine synthesis
Glycerophospholipid metabolism
Pentose phosphate pathway
CoA synthesis
Inositol phosphate metabolism
ROS detoxification
Taurine & hypotaurine metab.
Tyrosine metabolism
Sphingolipid metabolism
Nucleotide salvage pathway
Galactose metabolism
NAD metabolism
Fructose & mannose metabolism
Cholesterol metabolism
Arginine & proline metabolism
Pyruvate metabolism
Bile acid synthesis
Fatty acid synthesis
Tryptophan metabolism
Fatty acid oxidation
HMBS
UROS
UROD
CPOX
PPOX
PPAT
GART
PAICS
ATIC
PFAS
AFMID
KYNU
KMO
HAAO
freq. essentiality in parasitosomes [%]
G
HEPATOCYTE
PARASITE
ornithine
ODC1
CO2
putrescine
SRM
spermidine
SRM or SMS
spermine
AMD1
SAM
dcSAM
5MTA
Pf.AMD/ODC
Pf.SRM
H
require host-SRM
independent from host-SRM
5MTA
spermine
SAM
ornithine
dcSAM
SAM
spermidine
dcSAM
5MTA
putrescine
Nutrients
Products
I
SAM ↔ dcSAM
ornithine ↔ putrescine
putrescine ↔ spermidine
spermidine ↔ spermine
Active reaction
Non active reaction

Figure 2

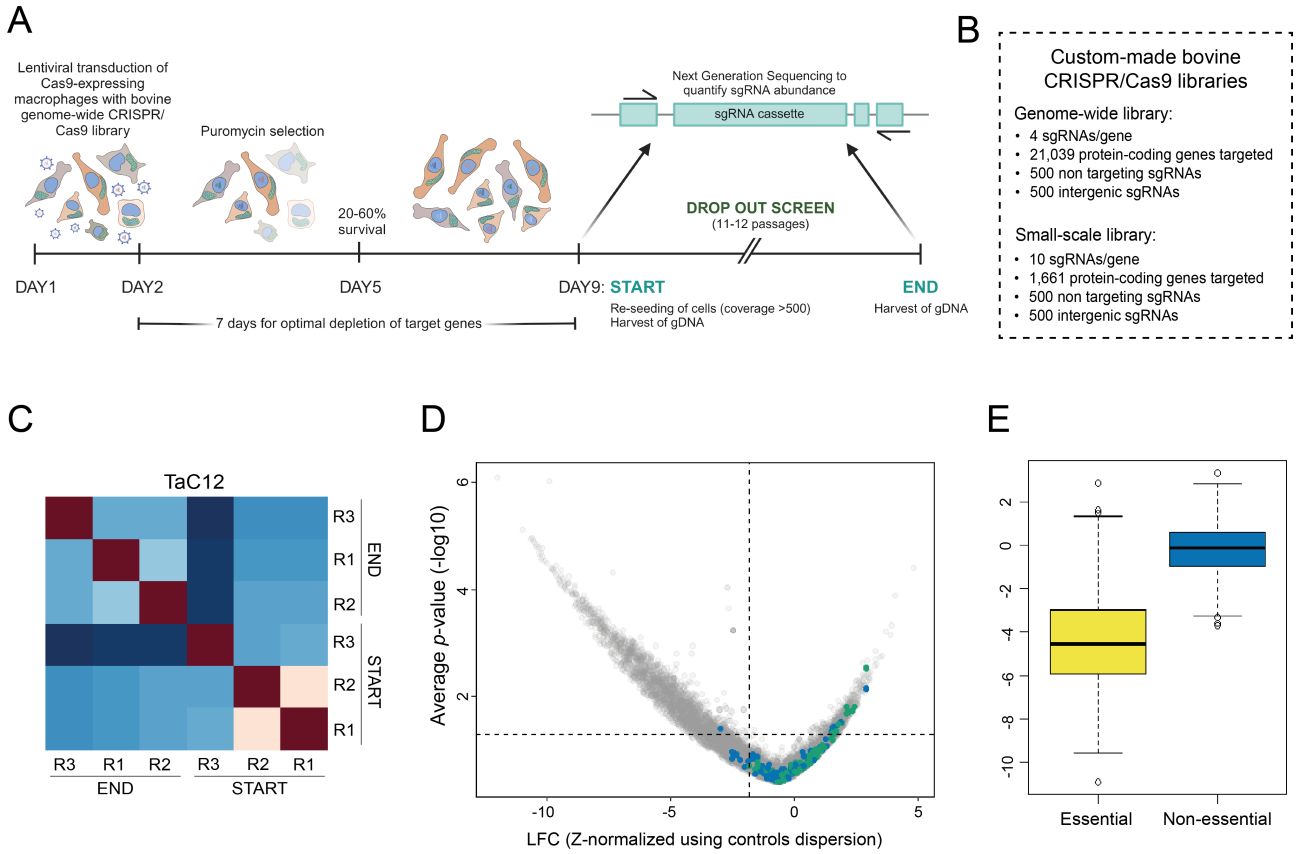
A
Lentiviral transduction of Cas9-expressing macrophages with bovine genome-wide CRISPR/ Cas9 library
Puromycin selection
20-60% survival
Next Generation Sequencing to quantify sgRNA abundance
sgRNA cassette
DROP OUT SCREEN
(11-12 passages)
DAY1
DAY2
DAY5
DAY9: START
END
Re-seeding of cells (coverage >500)
Harvest of gDNA
Harvest of gDNA
7 days for optimal depletion of target genes
B
Custom-made bovine CRISPR/Cas9 libraries
Genome-wide library:
• 4 sgRNAs/gene
• 21,039 protein-coding genes targeted
• 500 non targeting sgRNAs
• 500 intergenic sgRNAs
Small-scale library:
• 10 sgRNAs/gene
• 1,661 protein-coding genes targeted
• 500 non targeting sgRNAs
• 500 intergenic sgRNAs
C
TaC12
R3
R1
R2
END
R3
R2
R1
START
R3 R1 R2 R3 R2 R1
END
START
D
Average p-value (-log10)
LFC (Z-normalized using controls dispersion)
E
Essential
Non-essential

Figure 3

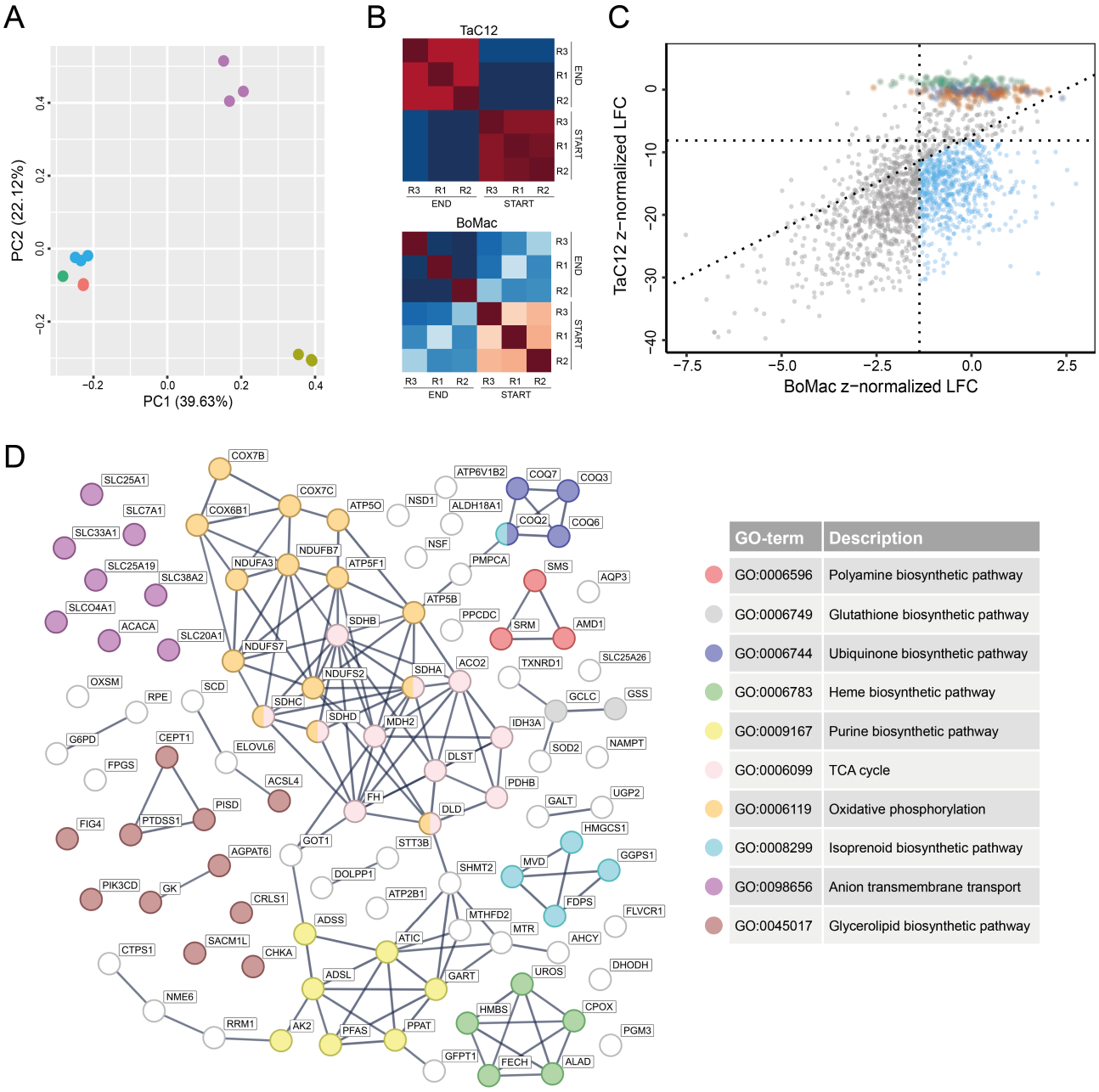
A
PC2 (22.12%)
PC1 (39.63%)
B
TaC12
BoMac
R3 R1 R2 R3 R1 R2
END
START
C
TaC12 z−normalized LFC
BoMac z−normalized LFC
D
GO-term
Description
GO:0006596 Polyamine biosynthetic pathway
GO:0006749 Glutathione biosynthetic pathway
GO:0006744 Ubiquinone biosynthetic pathway
GO:0006783 Heme biosynthetic pathway
GO:0009167 Purine biosynthetic pathway
GO:0006099 TCA cycle
GO:0006119 Oxidative phosphorylation
GO:0008299 Isoprenoid biosynthetic pathway
GO:0098656 Anion transmembrane transport
GO:0045017 Glycerolipid biosynthetic pathway

Figure 4

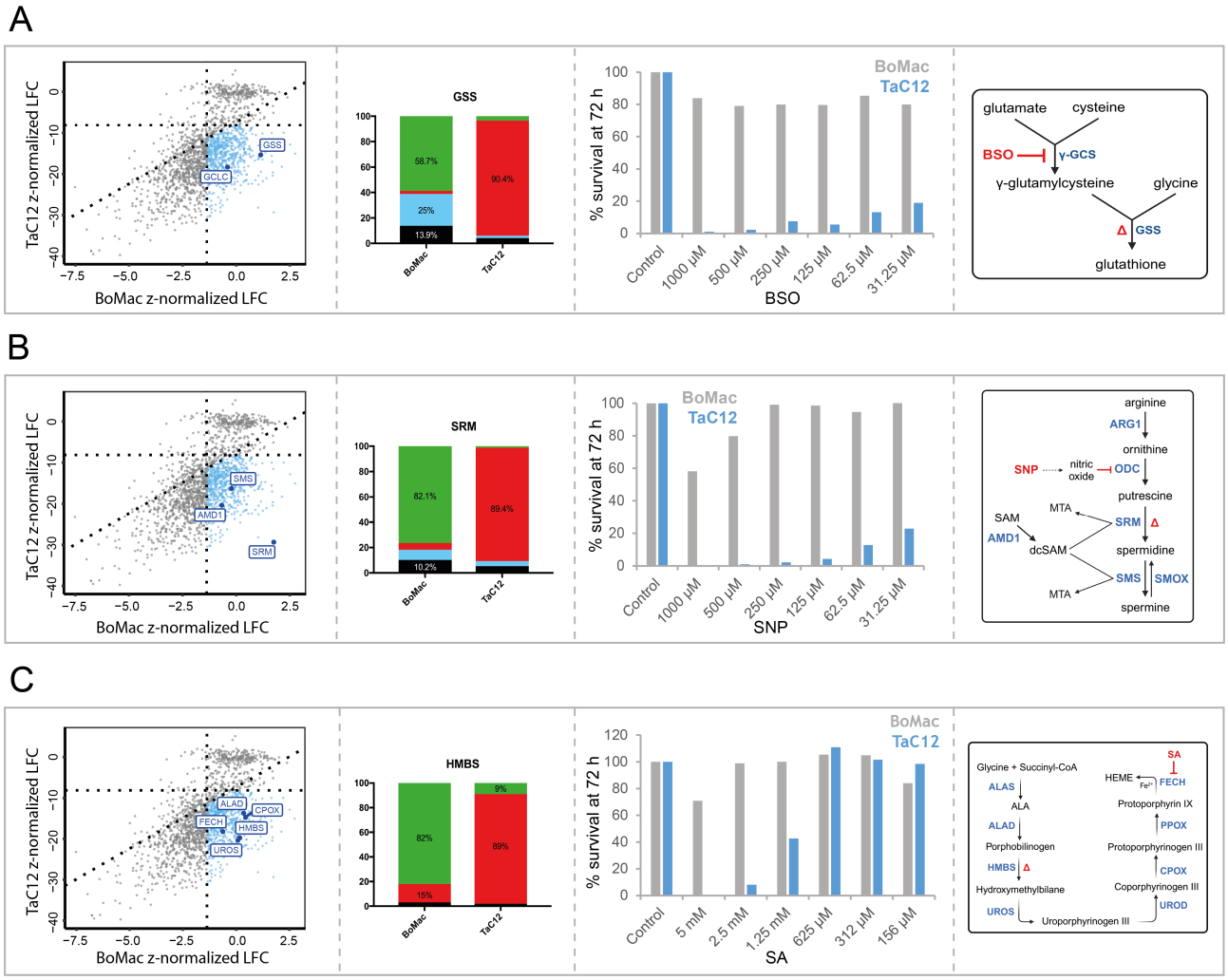
A
TaC12 z-normalized LFC
BoMac z-normalized LFC
GSS
GCLC
GSS
58.7%
25%
13.9%
90.4%
BoMac
TaC12
% survival at 72 h
BoMac
TaC12
Control
1000 µM
500 µM
250 µM
125 µM
62.5 µM
31.25 µM
BSO
glutamate
cysteine
BSO
γ-GCS
γ-glutamylcysteine
glycine
Δ
GSS
glutathione
B
SMS
AMD1
SRM
82.1%
10.2%
89.4%
SNP
arginine
ARG1
ornithine
SNP
nitric oxide
ODC
putrescine
MTA
SAM
AMD1
dcSAM
SRM
Δ
spermidine
SMS
SMOX
MTA
spermine
C
ALAD
CPOX
FECH
HMBS
UROS
82%
15%
9%
89%
SA
Glycine + Succinyl-CoA
ALAS
ALA
ALAD
Porphobilinogen
HMBS
Δ
Hydroxymethylbilane
UROS
Uroporphyrinogen III
HEME
Fe2+
FECH
SA
Protoporphyrin IX
PPOX
Protoporphyrinogen III
CPOX
Coporphyrinogen III
UROD

Figure 5

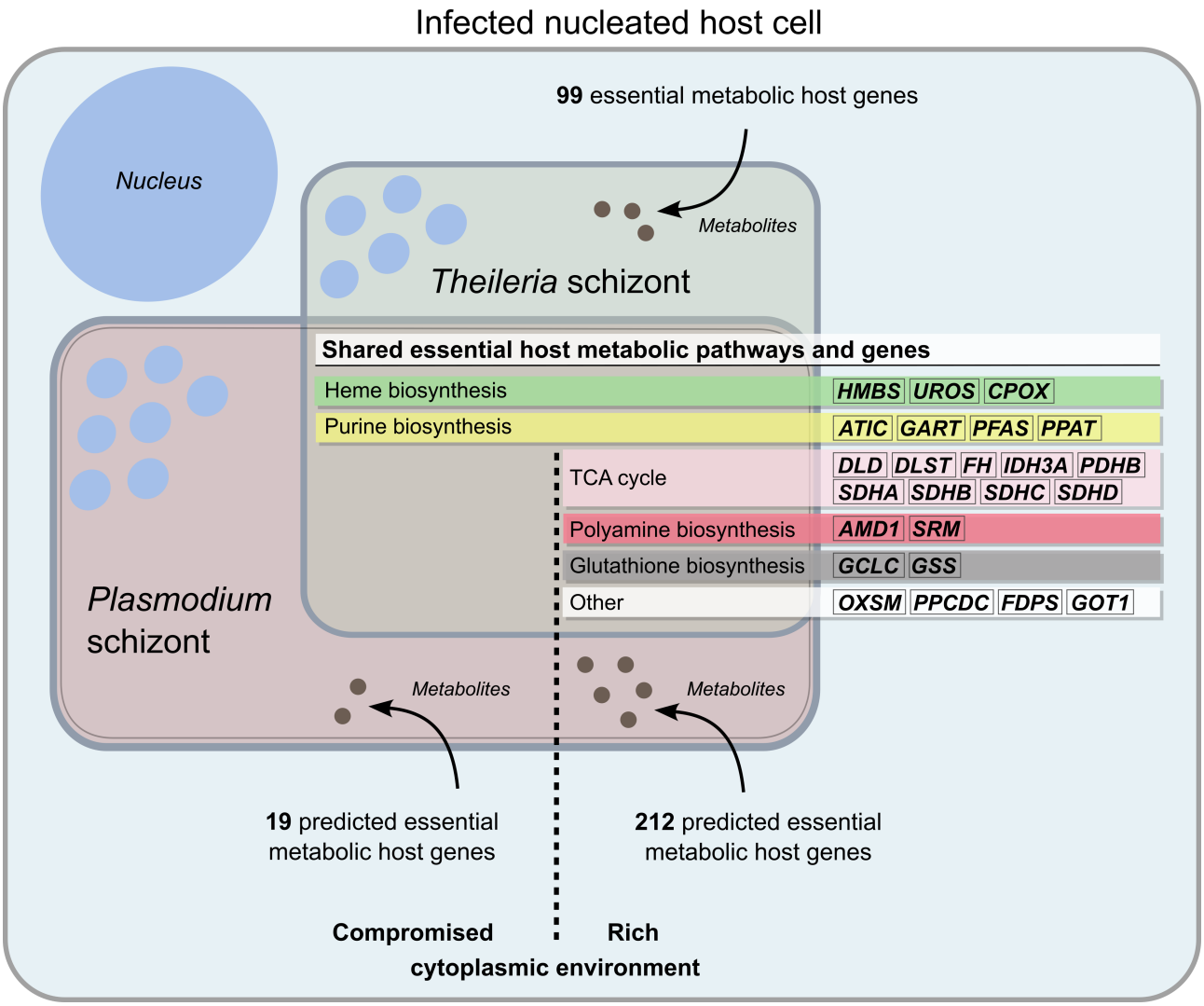
Infected nucleated host cell
99 essential metabolic host genes
Nucleus
Metabolites
Theileria schizont
Shared essential host metabolic pathways and genes
Heme biosynthesis
HMBS
UROS
CPOX
Purine biosynthesis
ATIC
GART
PFAS
PPAT
TCA cycle
DLD
DLST
FH
IDH3A
PDHB
SDHA
SDHB
SDHC
SDHD
Polyamine biosynthesis
AMD1
SRM
Glutathione biosynthesis
GCLC
GSS
Other
OXSM
PPCDC
FDPS
GOT1
Plasmodium schizont
Metabolites
Metabolites
19 predicted essential metabolic host genes
212 predicted essential metabolic host genes
Compromised
Rich
cytoplasmic environment

Figure 6

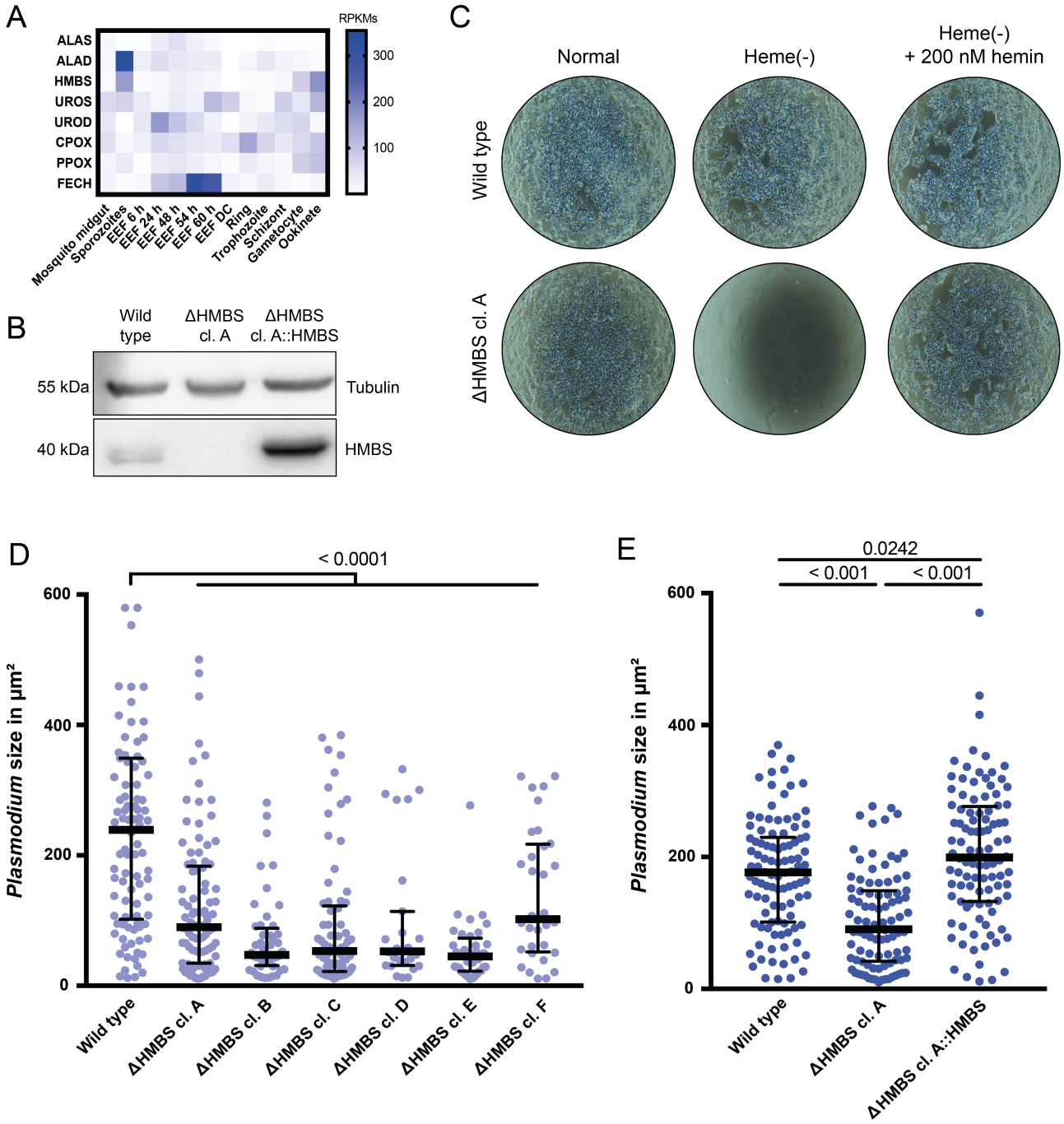

1337

1338 **Figure 7**